

Geological Society of America Bulletin

Structural evolution of the Gurla Mandhata detachment system, southwest Tibet: Implications for the eastward extent of the Karakoram fault system

M.A. Murphy, An Yin, P. Kapp, T.M. Harrison, C.E. Manning, F.J. Ryerson, Ding Lin and Guo Jinghui

Geological Society of America Bulletin 2002;114, no. 4;428-447
doi: 10.1130/0016-7606(2002)114<0428:SEOTGM>2.0.CO;2

Email alerting services

click www.gsapubs.org/cgi/alerts to receive free e-mail alerts when new articles cite this article

Subscribe

click www.gsapubs.org/subscriptions/ to subscribe to Geological Society of America Bulletin

Permission request

click <http://www.geosociety.org/pubs/copyrt.htm#gsa> to contact GSA

Copyright not claimed on content prepared wholly by U.S. government employees within scope of their employment. Individual scientists are hereby granted permission, without fees or further requests to GSA, to use a single figure, a single table, and/or a brief paragraph of text in subsequent works and to make unlimited copies of items in GSA's journals for noncommercial use in classrooms to further education and science. This file may not be posted to any Web site, but authors may post the abstracts only of their articles on their own or their organization's Web site providing the posting includes a reference to the article's full citation. GSA provides this and other forums for the presentation of diverse opinions and positions by scientists worldwide, regardless of their race, citizenship, gender, religion, or political viewpoint. Opinions presented in this publication do not reflect official positions of the Society.

Notes

Structural evolution of the Gurla Mandhata detachment system, southwest Tibet: Implications for the eastward extent of the Karakoram fault system

M.A. Murphy*

An Yin

P. Kapp†

T.M. Harrison

C.E. Manning

Department of Earth and Space Sciences and Institute of Geophysics and Planetary Physics, University of California, Los Angeles, California 90095-1567, USA

F.J. Ryerson

Lawrence Livermore National Laboratory, Livermore, California 94550, USA

Ding Lin

Guo Jinghui

Institute of Geology and Geophysics, Chinese Academy of Sciences, Beijing, China

ABSTRACT

Field mapping and geochronologic and thermobarometric analyses of the Gurla Mandhata area, in southwest Tibet, reveal major middle to late Miocene, east-west extension along a normal-fault system, termed the Gurla Mandhata detachment system. The maximum fault slip occurs along a pair of low-angle normal faults that have caused significant tectonic denudation of the Tethyan Sedimentary Sequence, resulting in juxtaposition of weakly metamorphosed Paleozoic rocks and Tertiary sedimentary rocks in the hanging wall over amphibolite-facies mylonitic schist, marble, gneisses, and variably deformed leucogranite bodies in the footwall. The footwall of the detachment fault system records a late Miocene intrusive event, in part contemporaneous with top-to-the-west ductile normal shearing. The consistency of the mean shear direction within the mylonitic footwall rocks and its correlation with structurally higher brittle normal faults suggest

that they represent an evolving low-angle normal-fault system. $^{40}\text{Ar}/^{39}\text{Ar}$ data from muscovite and biotite from the footwall rocks indicate that it cooled below 400 °C by ca. 9 Ma. Consideration of the original depth and dip angle of the detachment fault prior to exhumation of the footwall yields total slip estimates between 66 and 35 km across the Gurla Mandhata detachment system. The slip estimates and timing constraints on the Gurla Mandhata detachment system are comparable to those estimated on the right-slip Karakoram fault system, to which it is interpreted to be kinematically linked. Moreover, the mean shear-sense direction on both the Karakoram fault and the Gurla Mandhata detachment system overlap along the intersection line between the mean orientations of the faults, which further supports a kinematic association. If valid, this interpretation extends previous results that the Karakoram fault extends to mid-crustal depths.

Keywords: Himalayas, kinematics, metamorphic core complex, strike-slip faults, Tibetan plateau.

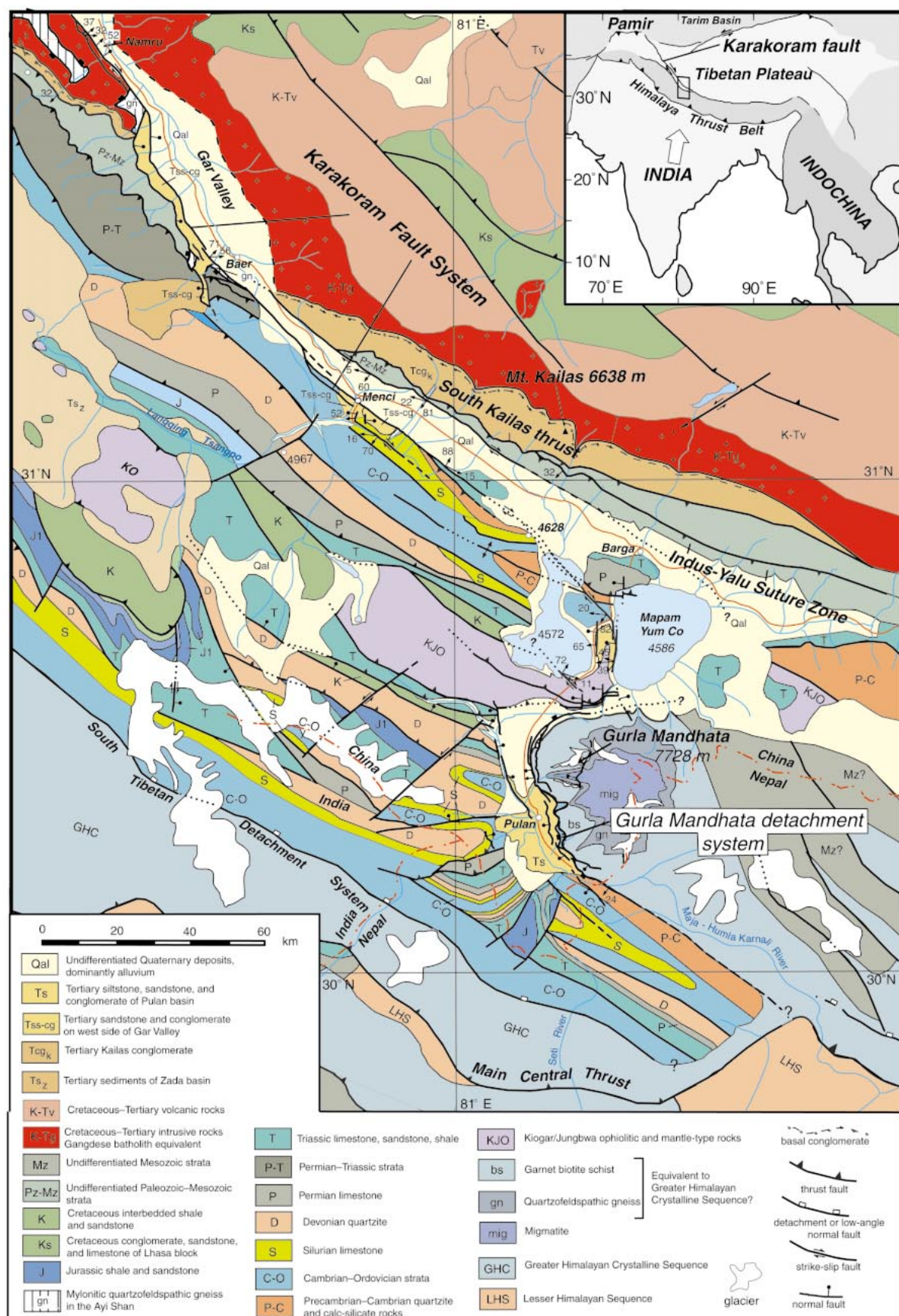
INTRODUCTION

The extent to which we can reconstruct orogenic systems is governed by how well the

boundaries between tectonically distinct domains are defined. Although several insightful studies have been conducted to understand the processes controlling contemporaneous east-west extension and distributed strike-slip faulting within the Tibetan plateau and north-south shortening in the Himalayan thrust belt (Armijo et al., 1989; Molnar and Lyon-Caen, 1989; Avouac and Tapponnier, 1993; Molnar et al., 1993; England and Molnar, 1997; McCaffrey and Nabelek, 1998; Seeber and Pécher, 1998; Yin et al., 1999a), the evolution and even location of the boundaries between these two structural regimes remain insufficiently understood to make quantitative reconstructions since the initial collision between India and Asia at ca. 50–70 Ma (Klootwijk et al., 1992; Rowley, 1996; Hodges, 2000; Yin and Harrison, 2000).

The boundary between the western Tibetan plateau and the Himalayan fold-and-thrust belt is defined by the Karakoram fault (Fig. 1). It

Figure 1. Simplified geologic map of southwest Tibet compiled from mapping by Augusto Gansser (Heim and Gansser, 1939), Tibetan Bureau of Geology and Mineral Resources (Cheng and Xu, 1987), Yin et al. (1999b), and our own observations.



has been previously proposed that the Karakoram fault system accommodates (1) northward indentation of the Pamir promontory (Tapponnier et al., 1981; Burtman and Molnar, 1993; Strecker et al., 1995; Searle, 1996), (2) radial expansion of the Himalayan arc (Molnar and Lyon-Caen, 1989; Ratschbacher et al., 1994; Seeber and Pêcher, 1998), and (3) eastward lateral extrusion of the Tibetan plateau (Tapponnier et al., 1982; Peltzer and Tapponnier, 1988; Armijo et al., 1989; Pêcher, 1991; Avouac and Tapponnier, 1993). Assessing the relationships between deformation of the regions emphasized in the three proposed causes of the movement along the Karakoram fault system continues to be problematic because of uncertainties in its initiation age, the net slip on it, and the location of its potential lateral continuation across the Himalayan-Tibetan orogen. From the southern Pamirs southward to Mount Kailas, the Karakoram fault is well delineated. East of Mount Kailas, however, the location of the fault is speculative (e.g., Armijo et al., 1989; Ratschbacher et al., 1994).

Hypotheses for the geometry and extent of the Karakoram fault system at its southeast end define two groups. Peltzer and Tapponnier (1988) proposed that the Karakoram fault system transfers slip to the Indus-Yalu suture zone in the Mount Kailas-Gurla Mandhata region and extends across the entire length of southern Tibet. Alternatively, Pêcher (1991) suggested that the Karakoram fault system links with the South Tibet detachment system. He noted a systematic deflection in the orientation of mineral-stretching lineations at the top of the Greater Himalayan Crystalline Sequence, which he interpreted to indicate a right-lateral shear. Opposing both of these interpretations is the view that the Karakoram fault system terminates into the north-trending Pulan basin adjacent to Gurla Mandhata (Ratschbacher et al., 1994) or merges and terminates into the Indus-Yalu suture zone in the Mount Kailas area (Searle, 1996) (Fig. 1). We have tested these different interpretations by combining field mapping with geochronologic and thermobarometric analyses of rocks in the Mount Kailas-Gurla Mandhata region, where the Karakoram fault system is postulated to either terminate or transfer slip farther to the east. Here, we document the existence of a large-scale normal-fault system, termed the Gurla Mandhata detachment system, which has exhumed mid-crustal rocks belonging to the Greater Himalayan Crystalline Sequence. We interpret the faults defining the Pulan basin to be genetically related to the Gurla Mandhata detachment system. Together they represent an evolving extensional fault system.

On the basis of timing constraints, kinematic data, and slip estimates for both faults, we advocate a kinematic link between the Karakoram fault system and the Gurla Mandhata detachment system.

Regional Geology

The Himalayan-Tibetan orogen is built upon a complex tectonic collage that was created by sequential accretion, from north to south, of several microcontinents, flysch complexes, and island arcs onto the southern margin of Eurasia since the early Paleozoic (Allègre et al., 1984; Chang et al., 1986; Şengör and Natal'in, 1996; Yin and Nie, 1996; Hodges, 2000; Yin and Harrison, 2000). From north to south, the major tectonic elements in central and south Tibet consist of a middle Paleozoic microcontinent known as the Kunlun block, a Permian-Lower Jurassic flysch sequence referred to as the Songpan Ganzi terrane, a middle Paleozoic-Jurassic microcontinent, referred to as the Qiangtang block, and a Paleozoic-Mesozoic microcontinent known as the Lhasa block (Allègre et al., 1984; Chang et al., 1986; Şengör and Natal'in, 1996; Murphy et al., 1997). Discontinuous belts of ultramafic rocks separate each of these tectonic elements and are interpreted to represent obducted oceanic crust now defining the suture between them (Allègre et al., 1984; Girardeau et al., 1984; Pearce and Deng, 1988). The final assembling of this Tibetan collage occurred with the docking of the Lhasa block in the Late Jurassic (Yin et al., 1988). Together with the previously accreted blocks, the Lhasa block constitutes the southern extent of Asia prior to accretion of the Indian subcontinent at ca. 60–50 Ma (Klootwijk et al., 1992; Rowley, 1996). The Indus-Yalu suture separates these accreted blocks from Indian subcontinent.

The Himalaya lies between the Indian shield to the south and the Indus-Yalu suture to the north. It consists of three lithotectonic units bounded by three north-dipping late Cenozoic fault systems: The Main Boundary thrust, the Main Central thrust, and the South Tibetan detachment system. The Lesser Himalaya is the structurally lowest slice. It is bounded at the base by the Main Boundary thrust and at the top by the Main Central thrust and consists of Middle Proterozoic metasedimentary, sedimentary, and volcanic rocks, and Cambrian-Ordovician granitic rocks (Parrish and Hodges, 1996). The Greater Himalaya Crystalline Sequence is bounded by the Main Central thrust below and the South Tibetan detachment fault above (Burg and

Chen, 1984; Burchfiel et al., 1992) (Fig. 1) and is composed of sedimentary, granitic, and volcanic rocks of Late Proterozoic-Early Cambrian age (Parrish and Hodges, 1996; DeCelles et al., 2000), which were metamorphosed in the Tertiary. The North (or Tethyan) Himalaya lies between the South Tibetan detachment system and the Indus-Yalu suture zone. It consists of upper Precambrian-lower Paleozoic sedimentary and metasedimentary rocks (Gansser, 1964; Yin et al., 1988; Garzanti, 1999) and thick Permian-Cretaceous continental-margin sequences (Cheng and Xu, 1987; Brookfield, 1993; Garzanti, 1999). The entire sequence is commonly referred to as the Tethyan Sedimentary Sequence.

The active trace of the Karakoram fault cuts obliquely across the Songpan-Ganzi terrane and the Qiangtang and Lhasa blocks; at the southeast end of the trace in the Mount Kailas-Gurla Mandhata region, the active trace of the fault cuts across the Indus-Yalu suture into the North Himalaya (Fig. 1). Four fault systems merge in this region: (1) the South Kailas thrust, the site of north-directed movement (Gansser, 1964; Yin et al., 1999b); (2) the Tethyan fold-and-thrust belt, the site of south-directed folding and offset; (3) the right-slip Karakoram fault; and (4) the down-to-the-west Gurla Mandhata detachment system.

Geologic Setting and Previous Work

The Mount Kailas area was first investigated by Augusto Gansser in 1935 (Heim and Gansser, 1939; Gansser, 1964), who recognized both a thrust system with south-directed slip involving the Tethyan Sedimentary Sequence and a thrust system with north-directed slip along the Indus-Yalu suture zone, referred to as the South Kailas thrust (Fig. 1). This area remained unmapped following Gansser's reconnaissance work until 1987 when the Tibetan Bureau of Geology and Mineral Resources completed a two-year mapping project at a scale of 1:1 000 000 (Cheng and Xu, 1987). Their work focused chiefly on regional stratigraphic and age correlation with south-central and southeastern Tibetan rocks. Since then, four geologic expeditions have been made to the Mount Kailas-Gurla Mandhata region (Ratschbacher et al., 1994; Miller et al., 1999; Yin et al., 1999b; Murphy et al., 2000). Miller et al. (1999) investigated the composition and age of volcanic rocks exposed in the Mapam Yum Co area (Fig. 1). Yin et al. (1999b) investigated the deformation history along the Indus-Yalu suture, focusing on the slip history of the South Kailas thrust. As mapped by Ratschbacher et al. (1994) and

Murphy et al. (2000), a system of active brittle right-slip faults belonging to the Karakoram fault system extend into Mapam Yum Co and La'nga Co areas, also known as Lakes Mansarovar and Rakshas, respectively (Fig. 2¹). What has remained uncertain is whether this fault system extends eastward past Mount Kailas adjacent to the Indus-Yalu suture zone or, instead, links to active east-west extensional structures immediately south of Mount Kailas.

Armijo et al. (1989) and Liu (1993) noted a significant east-west extensional component to the Karakoram fault system in Gar Valley (Fig. 1). Ratschbacher et al. (1994) extended these observations southward to the Pulan basin and interpreted that it is kinematically linked to the Karakoram fault system, which they postulated may terminate there. Although it is clear from the pattern of active seismicity (e.g., Chen and Molnar, 1983) that the Karakoram fault and faults bounding the Pulan basin are both active and most likely linked in a neotectonic sense (Ratschbacher et al., 1994), long-term (tens of millions of years) linkage of these faults remains undetermined because of poor constraints on net slip and timing of the two fault systems. Murphy et al. (2000) estimated 66 ± 5.5 km of dominantly right slip on the southern part of the Karakoram fault on the basis of the offset of the South Kailas thrust. Yin et al. (1999b) interpreted the South Kailas thrust to have been active at 13 Ma on the basis of thermal modeling of its footwall, which places an upper limit on the time of slip for the Karakoram fault. If the Karakoram fault is linked to extension in the Pulan basin, then this slip estimate and timing constraint require compatible estimates for basin bounding structures. However, the small size and uncertain age of the Pulan basin have made it difficult to feed such a large magnitude of slip into normal faults bordering the basin. We outline next the results of our field investigation of the Gurla Mandhata area that documents a previously unrecognized low-angle normal-fault system, referred to as the Gurla Mandhata detachment system.

GEOLOGY OF THE GURLA MANDHATA AREA

Rocks within the Gurla Mandhata area were mapped during the summers of 1995, 1997, and 1998 at a scale of 1:100 000 (Fig. 2). The geologic framework may be viewed as con-

sisting of four different components, each with a unique deformational history. They are, from west to east, the Tethyan fold-and-thrust belt, the Pulan basin, the two Gurla Mandhata detachment faults, and an extensional ductile shear zone directly below the Gurla Mandhata detachment faults (Fig. 3).

Tethyan Fold-and-Thrust Belt

Exposed in the western part of the study area is a fold-and-thrust belt with southward vergence and offset, which exposes a >9.1 -km-thick section of the Tethyan Sedimentary Sequence (Fig. 4A). It consists of Upper Proterozoic through Lower Cretaceous marine sedimentary to low-grade metasedimentary rocks (mainly quartzite and phyllite). A large thrust sheet composed of mantle-type rocks (norite, dunite, and harzburgite) is exposed along the southern edge of La'nga Co and Mapam Yum Co. Gansser (1964) refers to this package of rocks as the Kiogar-Jungbwa ophiolite. South of this thrust sheet, the style of folding varies from broad and concentric far from major thrusts to tight and overturned adjacent to them (Fig. 4B). The largest stratigraphic throw occurs along a north-dipping thrust ~ 10 km southwest of Pulan (Figs. 1 and 2). It places Ordovician phyllite in its hanging wall over Permian–Upper Jurassic strata in its footwall (Gansser, 1964; Cheng and Xu, 1987). Because thrust faults in our study area and adjacent areas in the fold-and-thrust belt along strike do not contain crystalline basement rocks in their hanging walls (Cheng and Xu, 1987) (Figs. 1 and 2), we interpret this part of the fold-and-thrust belt, south of the Kiogar (or Jungbwa) ophiolite, to be restricted to the Tethyan Sedimentary Sequence (Fig. 4B). However, because no subsurface data exist, we cannot rule out the possibility that the thrust faults involve structurally deeper rocks as suggested by field studies in Ladakh (Corfield and Searle, 2000) and south-central Tibet (Ratschbacher et al., 1994).

Pulan Basin

Deposited unconformably above the Tethyan Sedimentary Sequence is a >400 -m-thick section of Tertiary sedimentary rocks that define the Pulan basin (Fig. 3). The basin post-dates contractional deformation related to the Tethyan fold-and-thrust belt. The dimensions of the Pulan basin, as defined by the spatial extent of the basin sedimentary fill, are 40 km long by 12 km wide (Fig. 2). It forms a local topographic low, flanked on the east by the

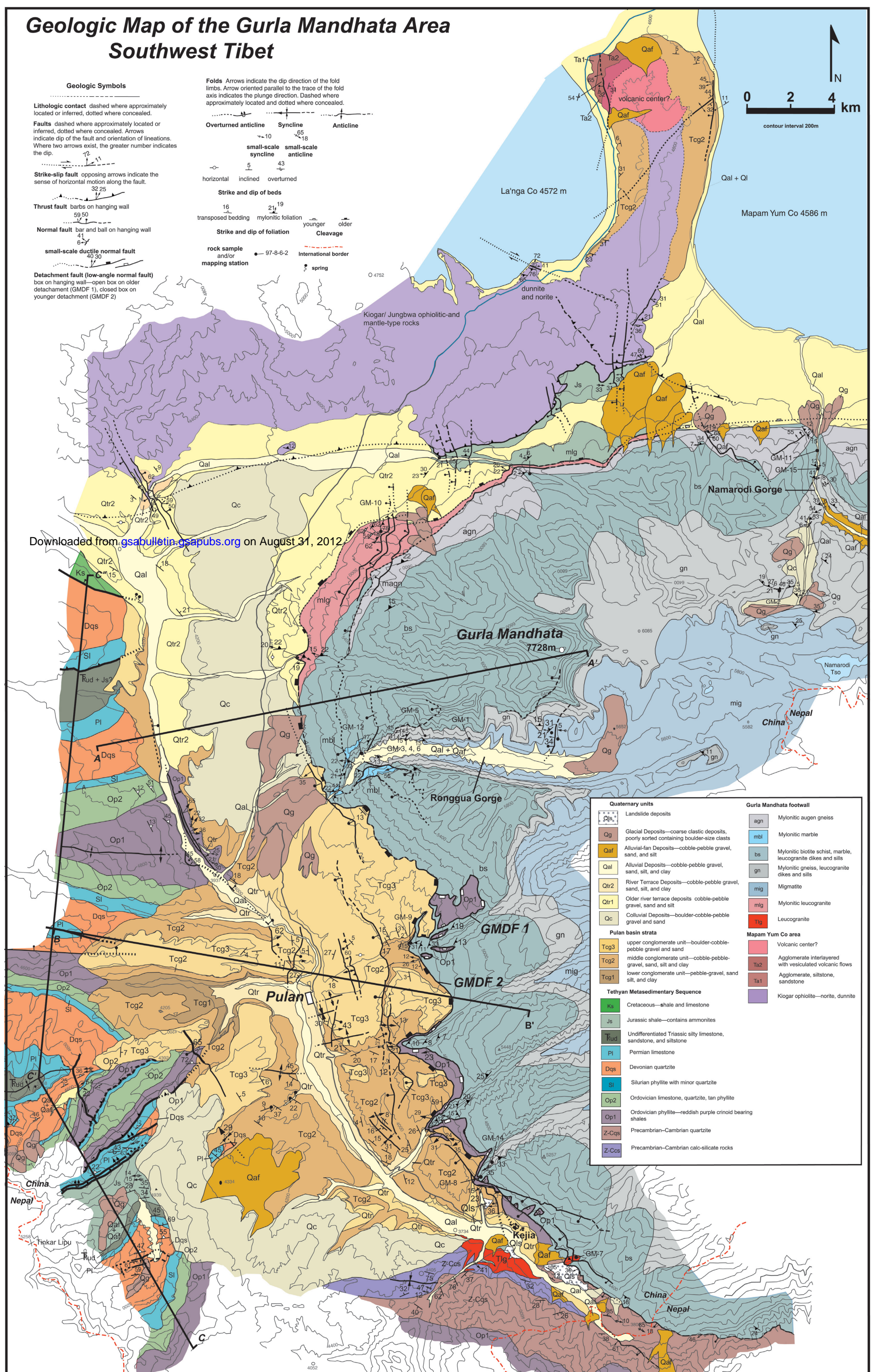
Gurla Mandhata peak (7728 m). The Maja River flows through the basin from north to south and slightly off center along its eastern margin, which in turn is connected to the Karnali River in far-western Nepal. Steeply to moderately dipping brittle normal faults bound the eastern and western margins of the basin.

The stratigraphy of the basin was investigated along seven east-west traverses along river-cut exposures. We divided the stratigraphy into three map units based on lithology and degree of deformation (Figs. 2 and 5A). The stratigraphically lowest unit (Tcg1) consists of interbedded white to tan sandstone and siltstone with minor pebble-gravel conglomerate lenses. Its thickness is >100 m. The base of the lower unit was not observed. Tcg1 is broadly folded along north-trending fold axes. Unconformably above Tcg1 lies an ~ 200 -m-thick, upward-coarsening sequence of white to tan sandstone, siltstone, and boulder-pebble conglomerates (Tcg2). The lower part of the sequence is dominated by interbedded siltstones and sandstones. Sandstone beds are fine- to medium-grained, poorly sorted, and 20–100 cm thick. Siltstone beds are 1–10 cm thick and contain plant debris. The upper part of the sequence is dominated by coarse-grained sandstone and boulder-cobble-pebble conglomerate. Conglomerate beds range from 1 to 2 m thick and are clast supported. Clasts are almost exclusively gneiss, leucogranite, and foliated leucogranite (Fig. 5B). Debris-flow deposits occur along the eastern margin of the basin within Tcg2 and are interpreted to have been deposited in an alluvial-fan environment. Both planar and trough cross-beds were observed in the finer-grained lithologies of the middle unit. The paleo-flow direction, as deduced from measurements of imbricated clasts, shows two preferred directions, south (175°) and west (261°) (Fig. 5C). The implied paleodrainage system with south- and west-flowing rivers is similar to the present drainage network (Fig. 2).

Capping Tcg2 is an ~ 100 -m-thick sequence of boulder-pebble conglomerate (Tcg3). The conglomerate is more completely lithified than the underlying Tcg2 unit and forms resistant ledges near Pulan. Although it contains a minor component of metamorphic clasts, it is dominated by clasts of sandstone and limestone (Fig. 5D). The paleo-flow direction, as deduced from measurements of imbricated pebbles, is dominantly eastward (Fig. 5E). Tcg3 dips homoclinally to the east at $\sim 5^\circ$. This unit defines a paleopenplain in the central and southern parts of the basin that has subsequently been incised by the Maja River.

¹Loose insert: Figure 2 is on a separate sheet accompanying this issue.

Geologic Map of the Gurla Mandhata Area Southwest Tibet



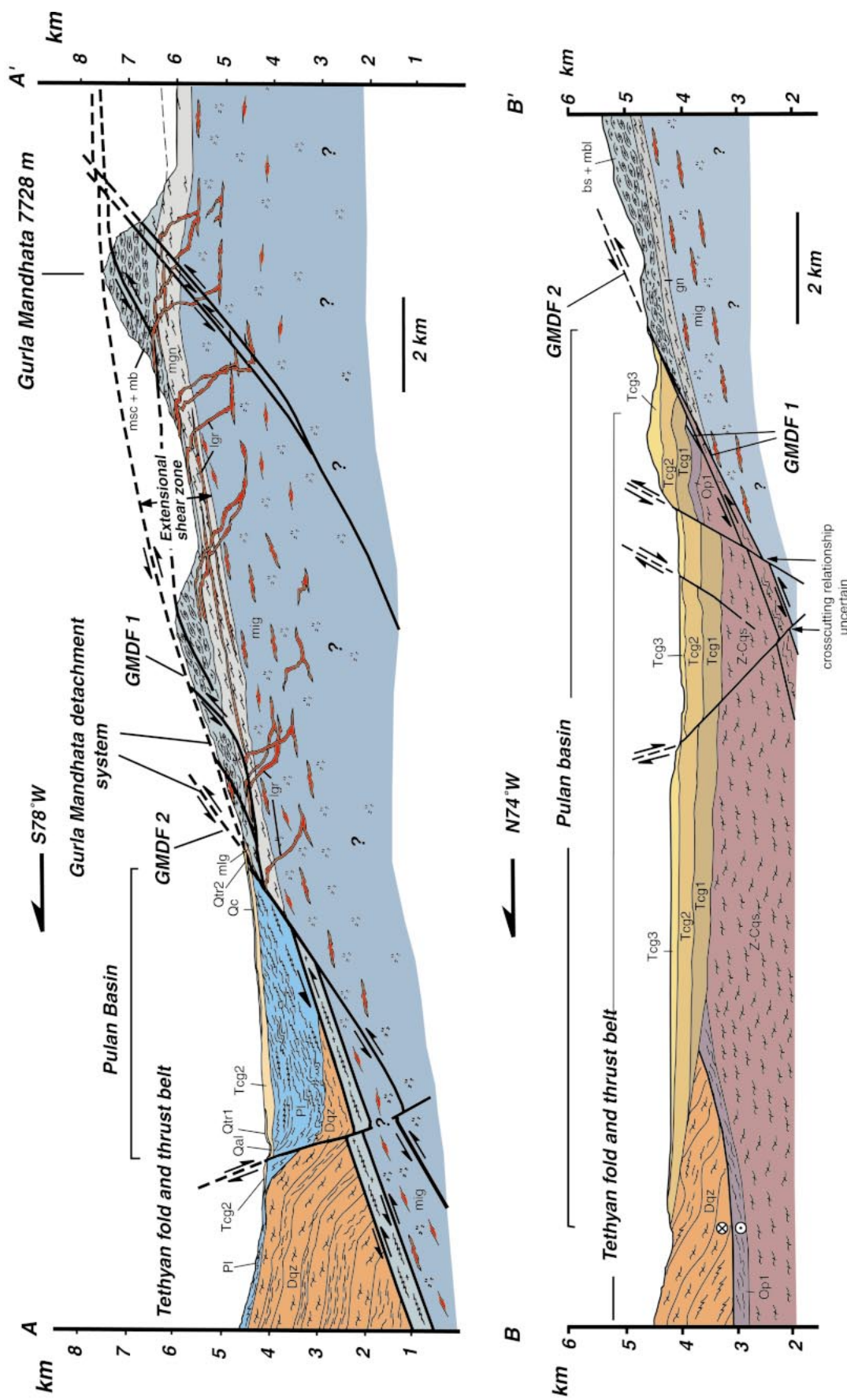
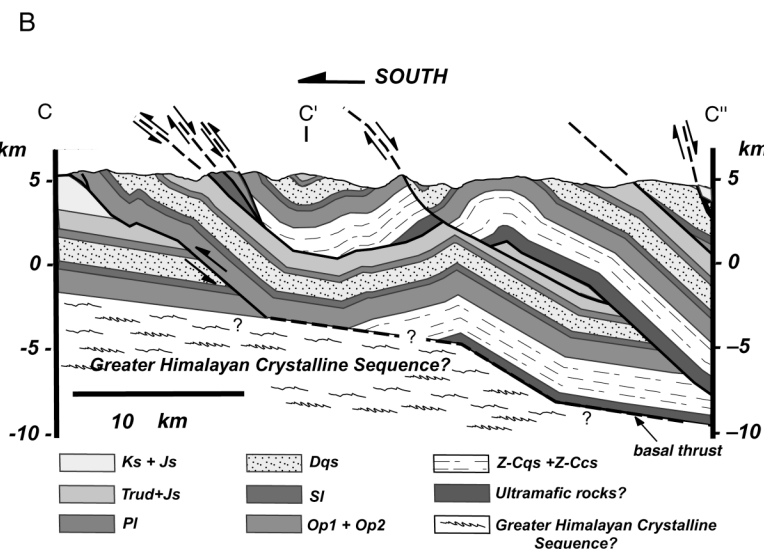
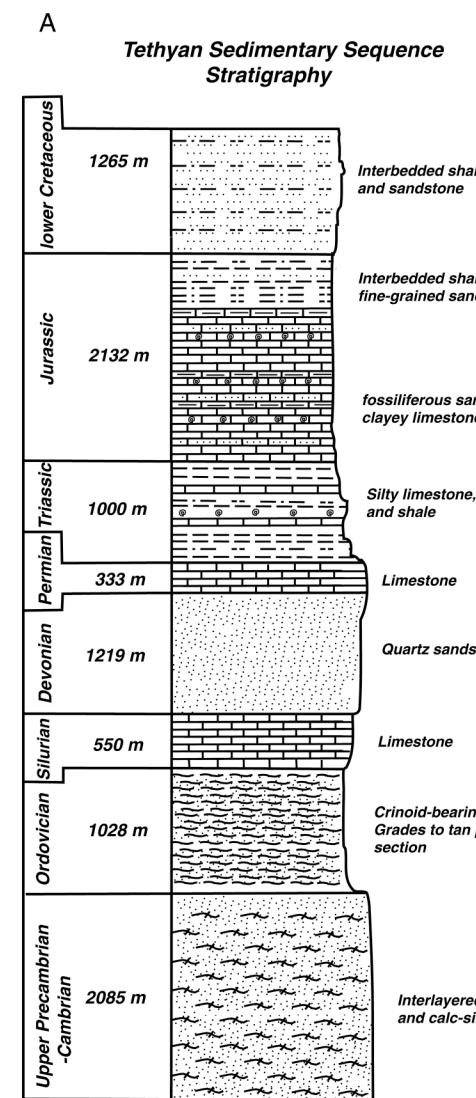


Figure 3. Geologic cross sections (A-A' and B-B') in the Gurla Mandhata area (see Fig. 2 for location). Qal—Quaternary alluvial deposits; Qtr2—younger Quaternary terrace deposits; Qtr3—older Quaternary terrace deposits; Tcg3—Tertiary conglomerate, upper unit of Pulan basin strata; Tcg2—Tertiary sedimentary rocks, middle unit of Pulan basin strata; Tcg1—Tertiary sedimentary rocks, lower unit of Pulan basin strata; Dqz—Devonian quartzite; Op1—Ordovician phyllite; Z-Cgs—Precambrian quartzite; mbl—marble; bs—mylonitic schist; gn—mylonitic gneiss; mig—migmatite; lgr—variably deformed leucogranite dikes and sills; mlg—mylonitic sill; GMDFA 1 and 2—Gurla Mandhata detachment faults 1 and 2. Leucogranite bodies are schematically shown to emphasize their crosscutting relationship.



The southern limit of exposed basin sedimentary fill is immediately south of Kejia near the China/Nepal border where a brittle normal-fault system defining the basin changes strike from a north trend to a more westerly orientation (Fig. 2).

North-trending normal faults broadly define the eastern and western limits of the Pulan basin strata (Fig. 2). The fault system consists of east- and west-dipping sets of discontinuous, subparallel normal faults (Fig. 6A). Both sets cut the upper Tcg3 unit of the Pulan basin strata (Tcg3). The east-dipping set can be traced ~20 km. Near Pulan, it branches into discontinuous en echelon normal faults (Fig. 2). The mean slip direction of the east-dipping fault set is $120^\circ \pm 20^\circ$ (Fig. 6B). The maximum stratigraphic throw, based on offset of the Tcg2/Tcg3 contact, is 150 m (Fig. 3; cross section B-B'). The west-dipping set is traceable for ~60 km from the southwest corner of Mapam Yum Co in the north to the town of Kejia in the south (Figs. 2 and 6A). Individual faults cannot be traced more than ~8 km. Together, these faults have a curved map pattern that closely follows the flanks of the Gurla Mandhata massif. The mean slip direction on these faults is $274^\circ \pm 10^\circ$ (Fig. 6B). The maximum stratigraphic throw, based on offset of the Tcg2/Tcg3 contact, is ~200 m. The magnitude of east-west extension of Tcg2 and Tcg3 is small, amounting to ~2% or 300 m (Fig. 3; cross section B-B'). The stratigraphically lowest unit (Tcg1) is clearly more deformed (Fig. 7A) and has probably been extended more. However, limited exposure of this unit precludes a quantitative estimate of its extensional strain.

Two fold sets—north-northwest trending and east-northeast trending—were observed in the Pulan basin sedimentary fill (Fig. 2). North-northwest-trending folds are spatially associated with north-northwest-trending normal faults and are interpreted to be related to slip on these faults possibly due to downdip bends in the fault surface. The north-trending fold in Figure 7A is interpreted as a rollover

Figure 4. (A) Stratigraphic column of the Tethyan Sedimentary Sequence in the Gurla Mandhata area, after Cheng and Xu (1987), Gansser (1964) and our own observations. (B) Cross section C-C' across the Tethyan fold-and-thrust belt (see Fig. 2 for location). Cross section is based on mapping by Heim and Gansser (1939) and our own observations. Lithologic symbols correlate to those in Figure 2.

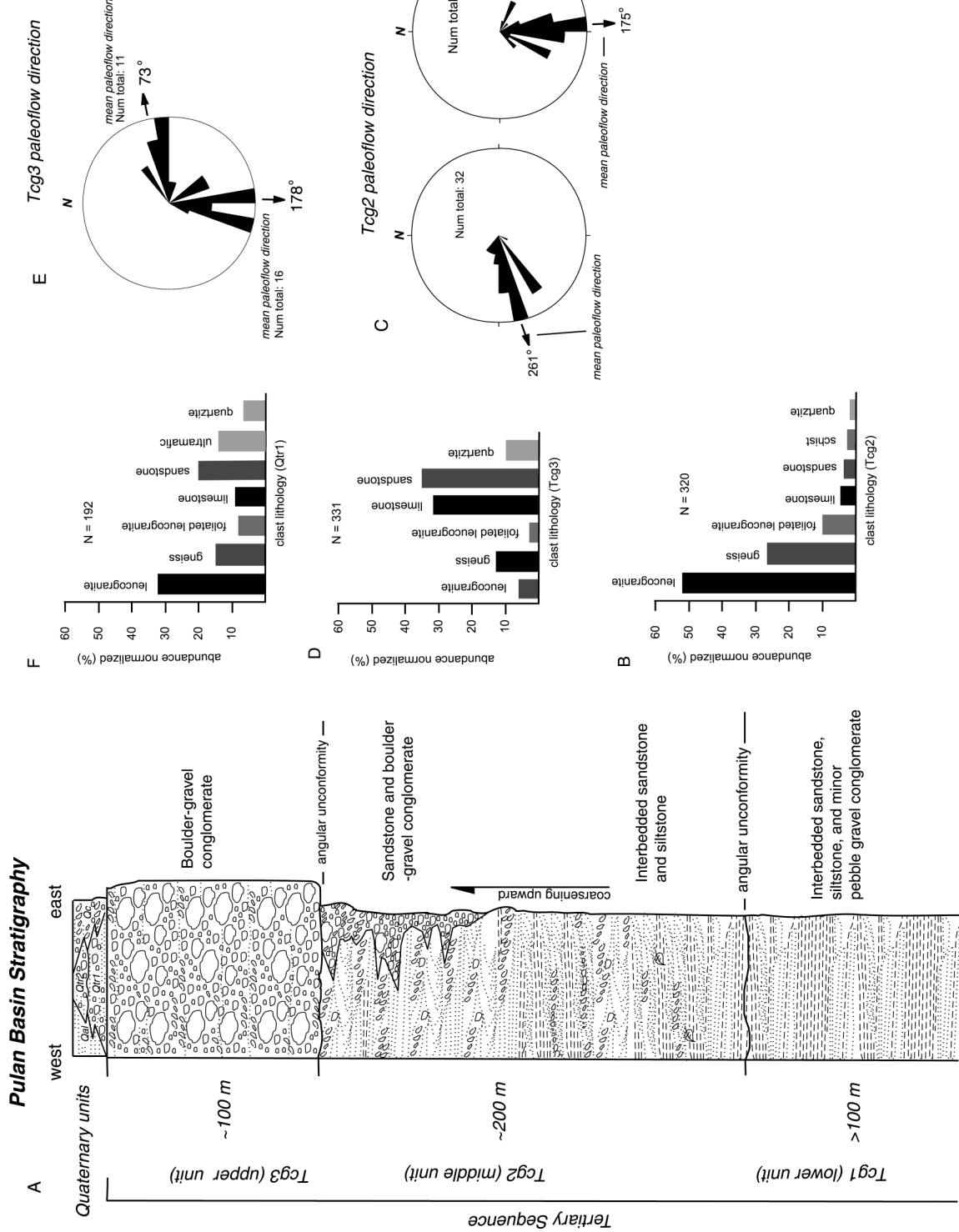
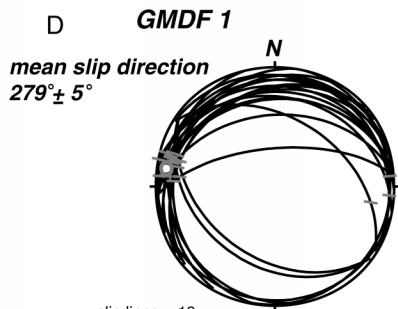
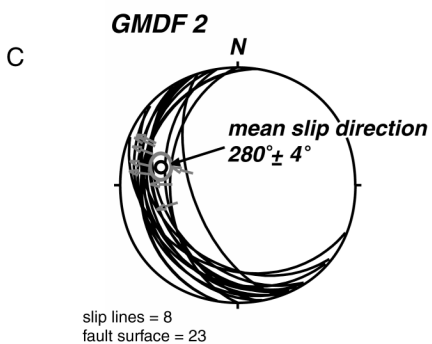
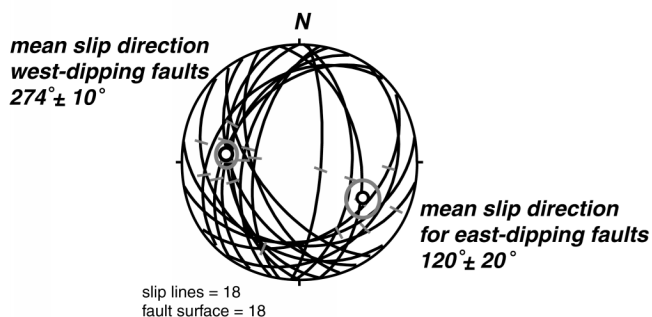
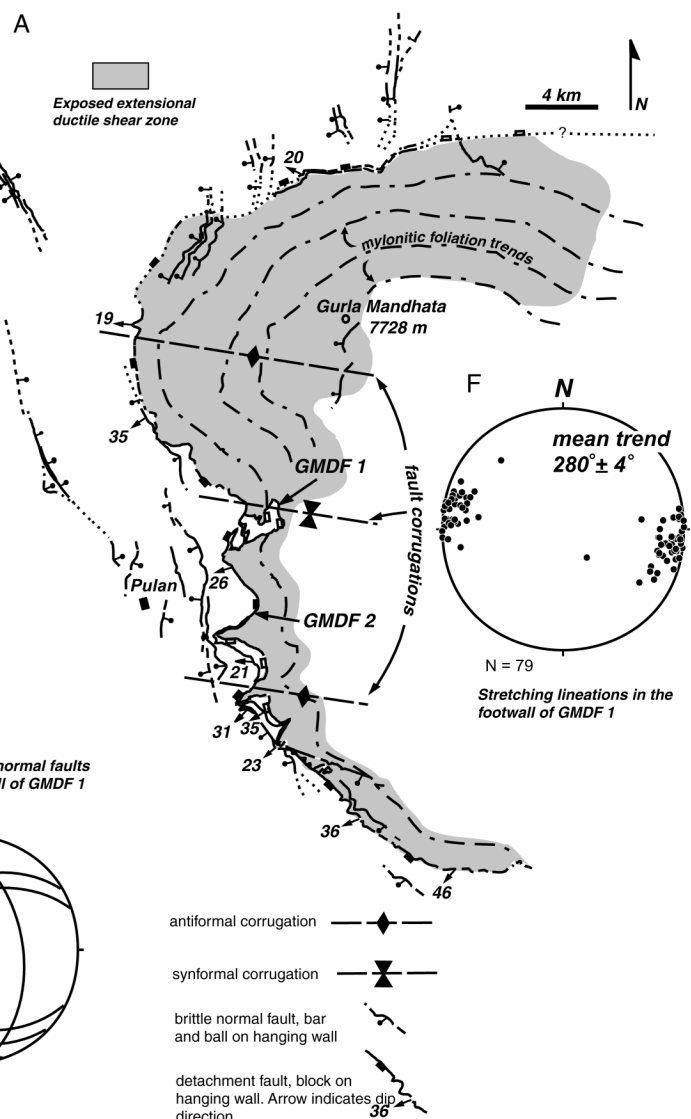
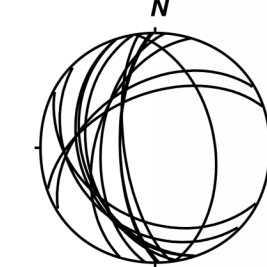


Figure 5. (A) Stratigraphic column of Pulan basin sedimentary rocks. Refer to Figure 3 for explanation of stratigraphic abbreviations. (B) Clast composition for Tcg2. (C) Two rose diagrams of paleoflow direction for middle unit deduced from imbricated pebbles measured at two localities. (D) Clast composition for Tcg3. (E) Rose diagram of paleoflow direction for Tcg3 deduced from imbricated pebbles. (F) Clast composition of Qtr1.

B Brittle normal faults (Pulan basin)

Orientation of ductile normal faults exposed in the footwall of GMDF 1

**Figure 6.** (A) Structure map of the Gurla Mandhata detachment system. (B–F) Lower-hemisphere, equal-area stereonet plots of structural data collected from the Gurla Mandhata detachment system.

structure, which implies that it formed by slip along a listric-shaped normal fault. East-northeast-trending folds are common near the tips of small magnitude (<200 m) north-trending normal faults (Fig. 2). We interpret these folds to reflect strain at accommodation zones between en echelon normal faults (e.g., Faulds and Varga, 1998).

Gurla Mandhata Detachment Faults

The eastern edge of the Pulan basin is bounded by a pair of west-dipping low-angle (<45°) normal faults, termed the Gurla Mandhata detachment fault 1 (older) and Gurla Mandhata detachment fault 2 (younger) (Fig.

7B). The curviplanar traces of both faults cross the flanks of the north, northwest, and west sides of the Gurla Mandhata massif (Fig. 2).

The structurally higher detachment, Gurla Mandhata detachment fault 2 (GMDF 2 in the figures), juxtaposes the lower (Tcg1) and middle (Tcg2) units of the Pulan basin in the fault's hanging wall against phyllite and marble in its footwall (Fig. 7A). Footwall units correlate with Ordovician rocks exposed to the west in the Tethyan fold-and-thrust belt (Fig. 2). Where exposed, the fault zone is defined by an ~2–10-cm-thick layer of foliated black, orange, and white clay gouge containing angular clasts of the footwall rocks. Well-

developed sets of P foliations and R₁ shears in the clay gouge indicate top-to-the-west shear (e.g., Rutter et al., 1986). Low strain is indicated by preserved crinoids in the rocks immediately beneath the detachment, but there is a weak stretching lineation that is defined by aligned muscovite and smeared quartz grains. Shear-sense direction on the fault was determined from tool marks, chatter marks, and P foliation–R₁ shear pairs in the clay gouge. The mean shear-sense direction on fault 2 is $280^\circ \pm 4^\circ$ (Fig. 6C).

Gurla Mandhata detachment fault 2 locally incises a structurally lower detachment fault, the Gurla Mandhata detachment fault 1 (GMDF 1 in the figures). The fault juxtaposes

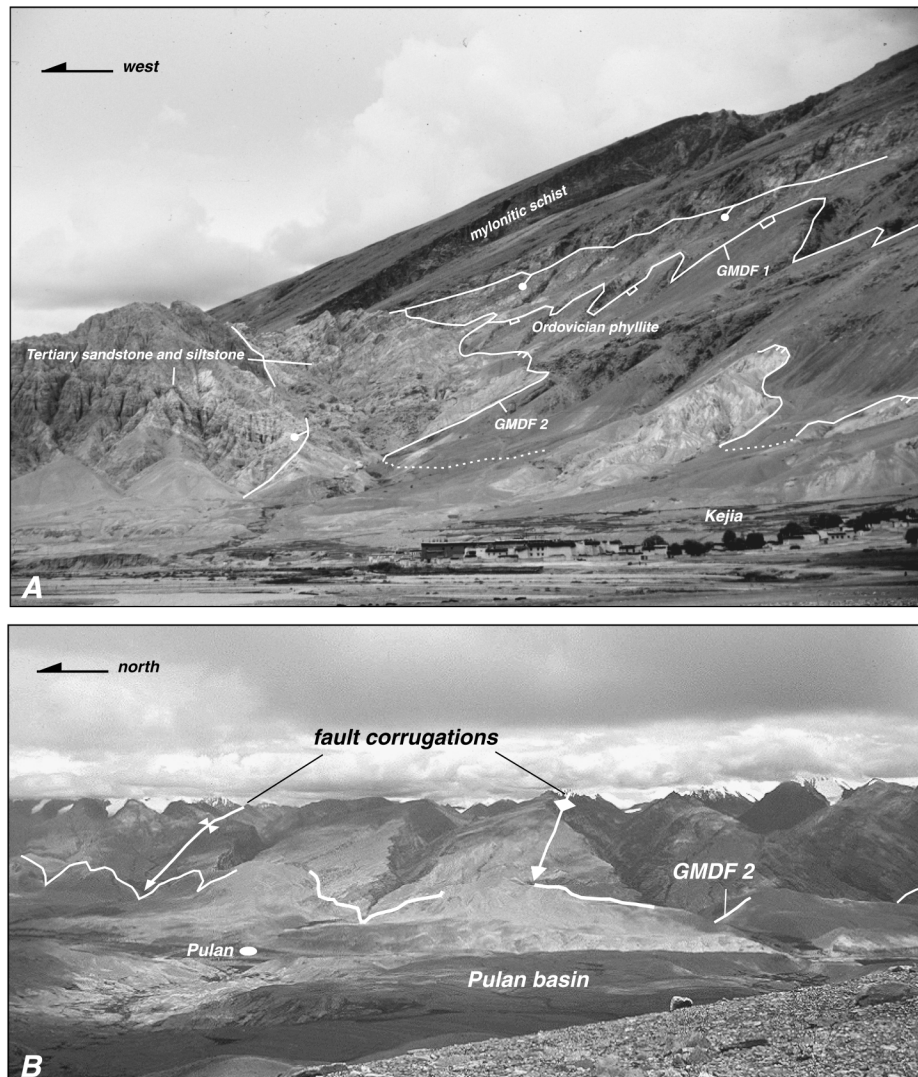


Figure 7. (A) Upper (younger) and lower (older) Gurla Mandhata detachment faults 1 and 2 (GMDF 1 and GMDF 2), respectively. View is to the north. Buildings in the center of the foreground are 5–10 m tall and lie ~1 km from the base of the mountain. Fault 2 juxtaposes the lower (Tcg1) and middle (Tcg2) stratigraphic units of the Pulan basin in the hanging wall against phyllite and marble in the footwall. Fault 1 places mylonitic schist, marble, gneiss, and variably deformed leucogranite dikes in the footwall against phyllite and marble in the hanging wall. Fault symbols: open box—GMDF 1, box on hanging wall; double-tick—GMDF 2, ticks on hanging wall; bar and ball—normal fault, bar and ball on hanging wall. (B) Eastern margin of the Pulan basin defined by the Gurla Mandhata detachment system. View is toward the east. The approximate width of field of view is 12 km.

lower Paleozoic phyllites and marbles in its hanging wall over a thick (>2 km) section of sillimanite-bearing mylonitic schists, gneisses, marbles, and variably deformed granite dikes and sills in its footwall. The hanging-wall rocks are commonly preserved as kilometer-scale klippen on the western lower slopes of the Gurla Mandhata massif. Where exposed, a sharp, striated contact defines the detachment.

Locally, a thin layer (<3 cm) of foliated, black-to-brown clay gouge with small angular mylonitic porphyroclasts derived from the footwall is present (Fig. 8A). In the footwall, immediately beneath this contact, is an ~2–5-m-thick cataclastic zone with calcite and epidote veins that overprint an older mylonitic foliation. Locally, fault 1 cuts this cataclastic zone and the footwall mylonitic foliation. Sev-

eral west-dipping and east-dipping, meter- to centimeter-scale brittle normal faults are present within this zone. Thin (~1–3 cm thick) cataclasite zones are present in this zone and lie subparallel to the attitude of the trace of fault 1. Often, they consist of a black aphanitic matrix (~80%) containing white feldspar porphyroclasts. The attitude of fault 1 partially defines a dome and in general dips ~18° to 30° away from the Gurla Mandhata massif (Fig. 6A). The mean shear-sense direction of fault 1 is $279^\circ \pm 5^\circ$ (Fig. 6D).

Footwall of the Gurla Mandhata Detachment System

The footwall rocks of the Gurla Mandhata detachment faults 1 and 2 were investigated along 11 traverses. Two traverses extended far into the footwall (~16 km) and were conducted in order to characterize the rock sequence and style of deformation. These two traverses are located in deeply incised valleys in the Gurla Mandhata massif (west side, Ronggua gorge; north side, Namariodi gorge) (Fig. 2). A 2.1-km-thick section of the footwall rocks is exposed along Ronggua gorge (Fig. 3; cross section A–A'), and in Namariodi gorge, an ~1-km-thick section is exposed. Immediately below fault 1 is a sequence of mylonitized garnet-biotite-muscovite schist (bs) and marble (mbl) that reaches a thickness of 1.2 km. Below this unit is an ~900-m-thick sequence of quartzofeldspathic biotite-garnet gneisses and biotite schist (gn). The structurally deepest rocks consist of quartzofeldspathic migmatitic gneiss (mig) that is >50 m thick. It consists of leucocratic bodies (elliptical bodies ~1–3 m in diameter and dikes up to 2 m thick), biotite-rich zones, and banded gneiss that contains a folded mylonitic fabric.

The characteristic mineral assemblage of the footwall rocks is (Bt + Ms + Grt + Plag + Sil). Inclusions in the garnet include biotite, plagioclase, muscovite, quartz, monazite, apatite, and ilmenite. Subhedral to anhedral garnets contain a nonrotational growth history and normally do not preserve a fabric.

Except for the migmatite unit, the entire sequence shares a common penetrative mylonitic fabric. Primary and secondary foliations (S, C, and C' foliations) are defined by aligned sillimanite (fibrolite), biotite, muscovite, and recrystallized quartz, whereas quartz rods, feldspar grains, and sillimanite grains define the lineation. The mean trend of the stretching lineations in the footwall rocks from the southwest, west, northwest, and north sides of the Gurla Mandhata massif is $280^\circ \pm 4^\circ$ (Fig. 6F). Several fabric elements in outcrop and in

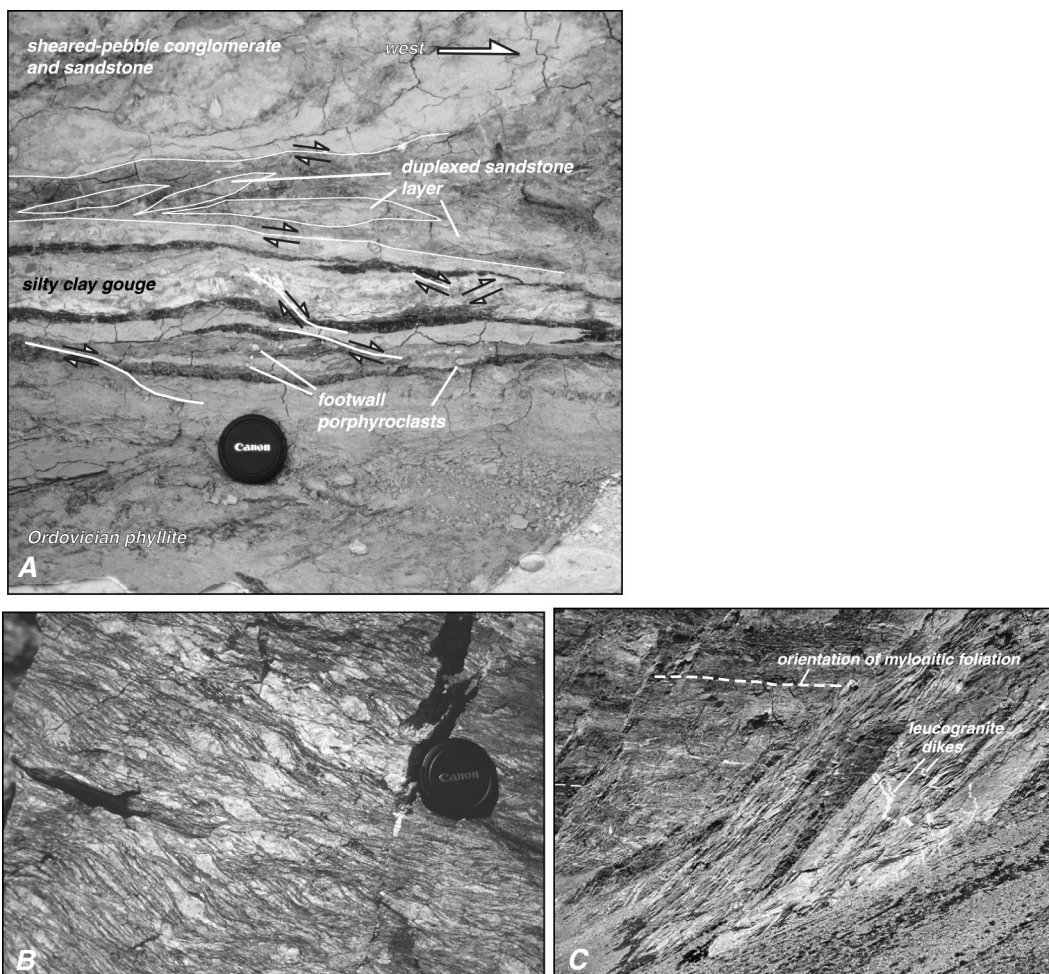


Figure 8. (A) Fault zone of Gurla Mandhata detachment fault 2, typified by sheared silty-clayey gouge exhibiting P foliations, R₁ shears, and top-to-the-west duplexes. View is toward the south. Photograph is taken from an outcrop immediately east of the town of Kejia. (B) Biotite-garnet gneiss in the footwall of the Gurla Mandhata detachment system in Namarodi gorge. View is toward the north. Note shear bands and asymmetric augen structures indicating west-directed shearing. (C) Cliff exposure along the north side of Ronggua gorge; 1–2-m-thick leucocratic granite dikes cut the mylonitic foliation at lower structural levels, but are deformed at higher structural levels and swing toward the west into parallelism with the shear zone. View to the north.

thin sections oriented parallel to lineation show asymmetry (asymmetric biotite and muscovite grains, domino-tilted and asymmetric feldspar grains and porphyroclasts, and shear banding), indicating a significant simple-shear component of deformation of the footwall (Fig. 8B). Most (~70%) indicate dominantly west-directed shearing in the footwall rocks, although some are consistent with top-to-the-east motion.

The most prominent structures in the footwall rocks are ductile normal faults. They exist at several scales, traceable for distances ranging from 10 cm to 1 km. Nearly all of these faults strike parallel to Gurla Mandhata detachment faults 1 and 2 (Fig. 6E) and display variable-slip magnitudes of tens of centimeters to hundreds of meters on the basis of

offset lithologic units. The largest of these is a top-to-the-west normal fault that cuts a 100-m-thick marble unit ~200–300 m below the detachment at the mouth of Ronggua gorge (Fig. 2).

The mylonitic foliation is folded at all scales. The most dominant folds are those with axes oriented subparallel to the stretching lineation, which we refer to as corrugations. The largest corrugations expressed in the mylonitic foliation, and by the traces of Gurla Mandhata detachment faults 1 and 2, have a wavelength of ~18 km (Figs. 6A and 7B). Fault 1 is commonly exposed in the core of synforms, suggesting that it had been folded more than the younger detachment (fault 2). Brittle normal faults along the eastern margin of the Pulan basin follow closely the curved

geometry of fault 1. The fact that these faults are not folded suggests they formed after the development of the corrugations.

The timing of formation of the east-trending folds (corrugations) is not clear. Three possibilities for the development of the folds are (1) the observed fold geometry could be inherited, possibly from north-south shortening related to the Tethyan fold-and-thrust belt; (2) the folding may also have developed synchronously with motion on the Gurla Mandhata detachment system in a constrictional strain field (e.g., Yin, 1991), and (3) they potentially developed late in the evolution of detachment faults 1 and 2. However, field observations favor that the corrugated fault geometry formed by north-south compression that was synchronous with east-west stretching. First, the im-

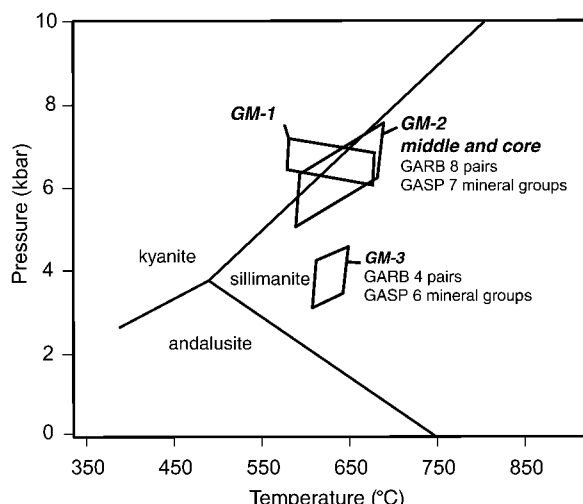


Figure 9. Thermobarometric results from rocks within the footwall of Gurla Mandhata detachment fault 1. Parallelograms indicate where pressure and temperature estimates from GARB and GASP overlap for a particular sample. Aluminum silicate stability field is after Holdaway (1971).

plied amplitude of the corrugations decreases with time, on the basis of (a) the crosscutting relationships between the mylonitic foliation and both detachment faults and (b) the preservation of fault 1-bounded klippen in the troughs of the synformal corrugations that fold the fault 2 surface. Second, the middle and upper units of the Pulan basin sedimentary rocks do not appear to be folded about axes parallel to the large-scale corrugations, suggesting that motion on the detachment occurred along a corrugated surface while the Pulan basin strata were being deposited. Third, the most extensive exposures of Pulan basin sedimentary rocks occur next to a synform, implying that this topographic depression existed during their deposition.

Footwall Leucogranites

Variably deformed leucogranite bodies make up ~10% to 20% of the footwall of Gurla Mandhata detachment fault 1. Five lithologies were recognized: (1) muscovite-bearing granite (2) muscovite-tourmaline-bearing granite (3) muscovite-biotite-bearing granite (4) biotite-bearing granite, and (5) biotite-garnet-bearing granite. We use the term “granite” to describe leucocratic ($\text{Qtz} + \text{K-feldspar} + \text{Plag}$) rocks in general. The most abundant lithology is muscovite-tourmaline-bearing granite, and the least abundant is biotite-garnet-bearing granite. Within the upper 2 km of the shear zone, leucogranite bodies occur exclusively as dikes and sills that are from tens of centimeters to 2 m thick. They gen-

erally display straight contacts with the country rock. In some cases, a tourmaline-rich zone is present along the contact between the dike and the country rock. Two generations of dikes and/or sills were recognized on the basis of their crosscutting relationship and intensity of deformation. The older set parallels the foliation and displays a mylonitic foliation similar to that of the country rock. The younger set cuts the older set at lower structural levels,

but is deformed at higher structural levels and swings toward the west into parallelism with the shear-zone foliation (Figs. 3 [cross section A-A'] and 8C). We interpret this relationship to indicate that the period of time between intrusion of the older and younger sets overlaps with top-to-the-west shearing.

THERMOBAROMETRY

Metamorphic pressures and temperatures were calculated for samples from the footwall rocks of the Gurla Mandhata detachment system by using the THERMOCALC computer program, version 2.75 (Powell and Holland, 1988), and the data set of Holland and Powell (1998). The plagioclase-garnet-Al₂SiO₅-quartz (GASP) barometer (Koziol and Newton, 1988) and the garnet-biotite (GARB) thermometer (Ferry and Spear, 1978) were used for the reported estimates (Fig. 9; GSA Data Repository item 1).² Sample locations are indicated in Figure 2. Mineral compositions were determined by using a Cameca Camebax electron microprobe at the University of California, Los Angeles (UCLA), with a nominal beam current of 10 nA and an accelerating voltage of 15 kV. Standardization was con-

²GSA Data Repository item 2002048, Mineral composition, trace element, and $^{40}\text{Ar}/^{39}\text{Ar}$ isotopic data, is available on the Web at <http://www.geosociety.org/pubs/ft2002.htm>. Requests may also be sent to editing@geosociety.org.

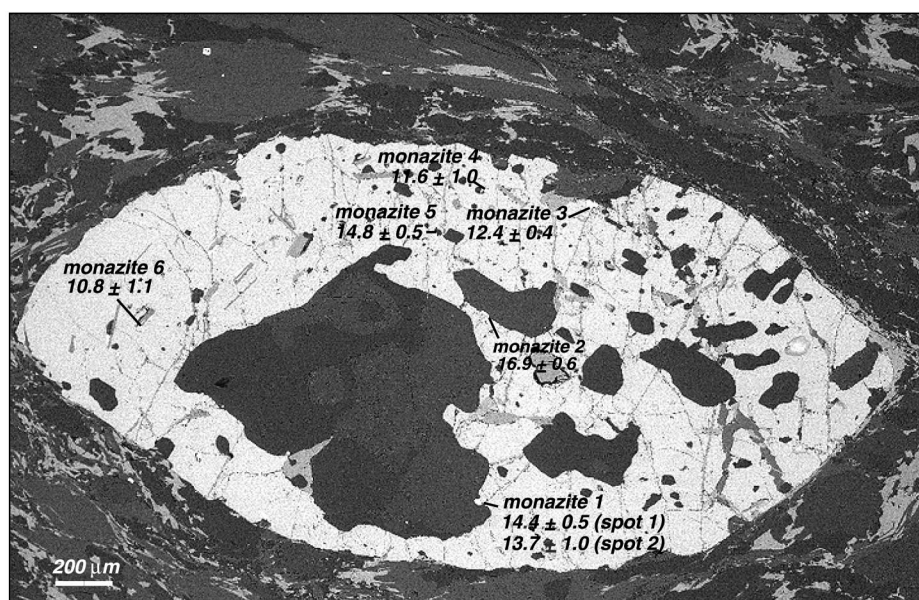


Figure 10. Backscattered-electron image showing textural relationship between monazite inclusions (dark) and garnet (light) in sample GM-3. Th-Pb monazite ages show a younging pattern from core to rim, which we interpret to reflect the age of garnet growth.

TABLE 1. Th-Pb ION-MICROPROBE MONAZITE AGES FOR GURLA MANDHATA SCHIST GM-3

Grain	Diameter (μm)	Spot	$^{208}\text{Pb}^*$ (%)	$^{208}\text{Pb}/^{232}\text{Th}$ age [†] (Ma $\pm 2\sigma$)
1	40		85	14.4 \pm 0.5
1	-	1	76	13.7 \pm 1.0
2	30	2	76	16.9 \pm 0.6
3	50	1	87	12.4 \pm 0.4
4	20	1	71	11.6 \pm 1.0
5	20	1	93	14.8 \pm 0.5
6	20	1	57	10.8 \pm 1.1
7	80	1	85	16.4 \pm 0.5
7	-	2	90	15.7 \pm 0.4
8	60	1	90	13.6 \pm 0.3
10	30	1	92	13.8 \pm 0.3
11	30	1	92	11.4 \pm 0.3

*Calculated by assuming common $^{208}\text{Pb}/^{204}\text{Pb}$ = 36.7.

[†]Ages based on comparison with monazite 554.

ducted on natural materials. Sillimanite and quartz were assumed to be pure phases.

Sample GM-1 is a garnet-biotite schist that contains garnet, anthophyllite, plagioclase, biotite, tourmaline, and quartz. Plagioclase, biotite, and quartz occur as inclusions in the garnet, whereas anthophyllite and tourmaline occur only in the matrix. If it is assumed that all were in equilibrium, the reaction anthophyllite + anorthite \rightarrow pyrope + grossular + quartz yields pressures between 6.5 and 7.5 kbar at temperatures between 550 and 650 °C (Fig. 9). The temperature is bracketed by biotite-garnet thermometry calculations (Ferry and Spear, 1978) and the given reaction. Both GM-2 and GM-3 are garnet-sillimanite-biotite-muscovite schists. Sample GM-2 lies ~200–300 m above the migmatite/gneiss contact, and GM-3 lies ~400–800 m above the same contact. X-ray mapping and electron-microprobe traverses of garnets in both samples show that they are homogeneous except near rims, which display strong increases in X_{sps} (spessartine component) and Fe/(Fe + Mg) and decreases in X_{alm} (almandine component) (GSA Data Repository item 2; see footnote 1). We interpret the rim composition as the result of diffusive zoning associated with declining temperature. Biotite-garnet thermometry (GARB) (Ferry and Spear, 1978) using biotite inclusions yields low temperature estimates between 390 and 450 °C for GM-3 and between 450 and 550 °C for GM-2. Sample GM-3 contains sillimanite, although these temperatures lie outside of the sillimanite stability field. Therefore, we conclude that biotite inclusions in the garnet are inappropriate for calculating peak temperatures. Instead, we have paired measurements of garnet-core compositions with those of matrix biotite crystals that lie on the order of a few millimeters from the garnet edge (Florence and

TABLE 2. Th-Pb ION-MICROPROBE ANALYSES OF GM-4 MONAZITE

Grain	Spot	$^{208}\text{Pb}^*/^{232}\text{Th}$ ($\times 10^{-4}$)	$^{208}\text{Pb}^*/^{232}\text{Th}$ ($\pm 1 \text{s.e.}$)($\times 10^{-6}$)	$^{208}\text{Pb}/^{204}\text{Pb}$	$^{208}\text{Pb}^*$ (%)	$^{208}\text{Pb}/^{232}\text{Th}$ age [†] (Ma $\pm 2\sigma$)
2	1	3.28	5.21	402	91	6.6 \pm 0.2
3	2	3.29	4.74	388	91	6.7 \pm 0.2
3	1	2.27	3.97	455	92	4.6 \pm 0.2
4	1	3.41	5.42	482	92	6.9 \pm 0.2
7	1	2.63	3.37	444	92	5.3 \pm 0.2
7	2	3.39	5.18	460	92	6.9 \pm 0.2
7	3	3.37	4.82	411	91	6.8 \pm 0.2
11	1	3.36	4.75	476	92	6.8 \pm 0.2

Note: s.e.—standard error.

*Calculated by assuming $^{208}\text{Pb}/^{204}\text{Pb}$ = 36.7.

[†]Ages based on comparison with monazite 554.

TABLE 3. Th-Pb ION-MICROPROBE ANALYSES OF GM-5 MONAZITE

Grain	Spot	$^{208}\text{Pb}^*/^{232}\text{Th}$ ($\times 10^{-4}$)	$^{208}\text{Pb}^*/^{232}\text{Th}$ ($\pm 1 \text{s.e.}$)($\times 10^{-6}$)	$^{208}\text{Pb}/^{204}\text{Pb}$	$^{208}\text{Pb}^*$ (%)	$^{208}\text{Pb}/^{232}\text{Th}$ age [†] (Ma $\pm 2\sigma$)
1	1	5.2	5.8	377	90	10.6 \pm 0.2
1	2	6.1	7.0	815	95	12.4 \pm 0.2
1	3	6.0	6.7	649	94	12.1 \pm 0.2
3	1	5.5	6.6	679	95	11.1 \pm 0.2
4	1	5.9	5.9	737	95	12.0 \pm 0.2
5	1	4.7	7.0	501	93	9.4 \pm 0.2
6	1	5.3	7.0	642	94	10.8 \pm 0.2
7	1	5.3	6.9	611	94	10.7 \pm 0.2
7	2	4.5	25	753	95	9.1 \pm 1.0
8	1	6.1	9.5	725	95	12.3 \pm 0.4
8	2	6.0	41	1089	97	12.0 \pm 1.6
9	1	5.6	6.1	657	94	11.4 \pm 0.2
11	1	6.1	7.1	560	93	12.3 \pm 0.2
12	1	5.7	6.3	652	94	11.4 \pm 0.2
12	2	6.2	59	1172	97	12.5 \pm 2.4
13	1	5.8	7.3	615	94	11.7 \pm 0.2
13	2	6.2	18	898	96	12.6 \pm 0.8

Note: s.e.—standard error.

*Calculated by assuming $^{208}\text{Pb}/^{204}\text{Pb}$ = 36.7.

[†]Ages based on comparison with monazite 554.

TABLE 4. Th-Pb ION-MICROPROBE ANALYSES OF GM-6 MONAZITE

Grain	Spot	$^{208}\text{Pb}^*/^{232}\text{Th}$ ($\times 10^{-4}$)	$^{208}\text{Pb}^*/^{232}\text{Th}$ ($\pm 1 \text{s.e.}$)($\times 10^{-6}$)	$^{208}\text{Pb}/^{204}\text{Pb}$	$^{208}\text{Pb}^*$ (%)	$^{208}\text{Pb}/^{232}\text{Th}$ age [†] (Ma $\pm 2\sigma$)
1	1	4.07	7.27	413	91	8.2 \pm 0.2
1	2	4.15	7.39	526	93	8.4 \pm 0.2
1	3	3.96	6.84	377	90	8.0 \pm 0.2
2	1	3.68	7.44	357	90	7.4 \pm 0.4
2	2	3.72	6.81	501	93	7.5 \pm 0.2
3	1	3.57	8.20	375	90	7.2 \pm 0.4
3	2	3.67	7.75	616	94	7.4 \pm 0.4
4	1	5.44	7.89	484	92	11.0 \pm 0.4
4	2	5.25	7.02	681	95	10.6 \pm 0.2
5	1	5.11	6.55	450	92	10.3 \pm 0.2
5	2	4.55	7.10	389	91	9.2 \pm 0.2
5	3	4.43	5.47	653	94	8.9 \pm 0.2
7	1	4.01	5.65	544	93	8.1 \pm 0.2

Note: s.e.—standard error.

*Calculated by assuming $^{208}\text{Pb}/^{204}\text{Pb}$ = 36.7.

[†]Ages based on comparison with monazite 554.

Spear, 1992). We should note that the proportion of garnet to biotite in rock is very small. Therefore, we would not expect that the biotite in the matrix has been significantly altered by net-transfer reactions involving the dissolution of garnet (Spear, 1993). GARB calculations using these pairs yield temperatures that we interpret to more accurately reflect the

peak temperature the rock was subjected to, given the degree of zoning observed (Florence and Spear, 1992) and the presence of sillimanite in both rocks. GASP (Koziol and Newton, 1988) calculations for GM-2 yield pressure estimates between 5 and 7.6 kbar in a temperature range defined by GARB calculations between 575 °C and 690 °C (Fig. 9). This result

is similar to the conditions estimated for GM-1. GASP and GARB calculations for GM-3 yielded pressures between 3.6 and 4.5 kbar and temperatures of 600 °C to 650 °C (Fig. 9). These results indicate that GM-2 and GM-1 equilibrated at ~2–3 kbar higher pressure than GM-3. Given that these two samples are now only ~500 m apart, perpendicular to the shear zone, we interpret this result to indicate that the footwall sequence was highly attenuated during shearing.

Age Constraints

To address the timing of metamorphism we undertook *in situ* Th-Pb dating of monazite that occurs as both inclusions in garnet (Fig. 10) and in the matrix of sample GM-3 (Table 1). Ten monazite grains identified in a polished thin section were dated *in situ* by the $^{208}\text{Pb}/^{232}\text{Th}$ ion-microprobe method described in Harrison et al. (1995). A single garnet grain containing six monazite inclusions and four additional monazite grains in the adjacent matrix were mounted with a standard in epoxy and Au coated for analysis. Analyses were conducted with an O⁻ primary beam focused to an ~20 μm spot. Ages are determined by direct reference to monazite standard 554 (Harrison et al., 1999). Monazite inclusions in sample GM-3 yielded a range of ages from 16.9 ± 0.3 Ma to 10.8 ± 0.6 Ma (Table 1) that show an apparent correspondence to their position within the garnet from core to rim (Fig. 10). Monazite grains in the matrix also show a range of ages between 16.5 and 11.5 Ma, a distribution of ages similar to that within the garnet. Interpreting these data as crystallization ages requires some consideration for the potential degree of Pb* (radiogenic Pb) loss. GARB thermometry indicates that GM-3 was subjected to temperatures of 600 to 650 °C. We do not think that the monazites have had significant Pb* loss for two reasons: (1) Both monazite inclusions and matrix monazites yield a similar spread in $^{208}\text{Pb}/^{232}\text{Th}$ ages, and none in the matrix are younger than those in the garnet; (2) Ar-closure ages of nearby biotites and muscovites imply that GM-3 has been at <400 °C since ca. 8.8 Ma, precluding the possibility of Pb* loss since that time (Smith and Giletti, 1997).

To ascertain the age relationships among the different leucogranite bodies, we dated (1) two dikes that cut the mylonitic foliation at deep structural levels, but are deformed and oriented parallel to the foliation higher in the shear zone (GM-4 [Table 2] and GM-5 [Table 3]), (2) a mylonitized sill (GM-6 [Table 4]) that is cut by GM-4, and (3) a mylonitized sill

TABLE 5. Th-Pb ION-MICROPROBE DATA OF GM-7 MONAZITE

Grain	Spot	$^{208}\text{Pb}^*/^{232}\text{Th}$ ($\times 10^{-4}$)	$^{208}\text{Pb}^*/^{232}\text{Th}$ (± 1 s.e.)($\times 10^{-6}$)	$^{208}\text{Pb}/^{204}\text{Pb}$	$^{208}\text{Pb}^*$ (%)	$^{208}\text{Pb}/^{232}\text{Th}$ age ^t (Ma $\pm 2\sigma$)
4	1	1.05	1.89	598	94	21.2 ± 0.8
4	2	1.01	3.91	742	95	20.5 ± 1.6
5	1	1.13	2.21	827	96	22.9 ± 0.8
5	2	0.89	3.33	948	96	18.0 ± 1.4
6	1	1.14	2.18	939	96	23.0 ± 0.8
7	1	0.94	1.12	769	95	18.9 ± 0.4
9	1	0.47	1.88	190	81	9.5 ± 0.8
10	1	0.64	2.41	194	81	12.9 ± 1.0
10	2	1.18	2.37	856	96	23.8 ± 1.0
12	1	0.86	1.95	694	95	17.4 ± 0.8
12	2	0.85	6.60	1172	97	17.2 ± 2.6

Note: s.e.—standard error.

*Calculated by assuming $^{208}\text{Pb}/^{204}\text{Pb} = 36.7$.

^tAges based on comparison with monazite 554.

(GM-7 [Table 5]) near the top of the footwall extensional shear zone, immediately beneath Gurla Mandhata detachment fault 1 (see Fig. 2 for sample location). All the granite bodies are small, <1 m thick, except for GM-7 that is ~30 m thick. We obtained $^{208}\text{Pb}/^{232}\text{Th}$ ion-microprobe monazite ages following the method described by Harrison et al. (1995). For each sample, ~8–20 grains of monazite were separated from 1 kg of rock by using standard rock-crushing and mineral-separation techniques and were mounted in epoxy with a monazite standard (554) and Au coated.

With the exception of GM-7, all monazites analyzed yield an early to late Miocene age peak. However, interpretation of the data is complicated owing to a relatively wide range of ages that is observed in every sample. Sample GM-4 (Table 2) yields a weighted mean age of 6.8 ± 0.2 Ma with an MSWD (mean square of weighted deviates) of 0.97, excluding two repeat spot analyses on grains 3 and 7. GM-4 is a sample of a dike with an orientation of N20°W/65°NE. A nearby sill (sample GM-6 [Table 4]), which is cut by the GM-4 dike, yields a weighted mean age of $8.7 \pm$

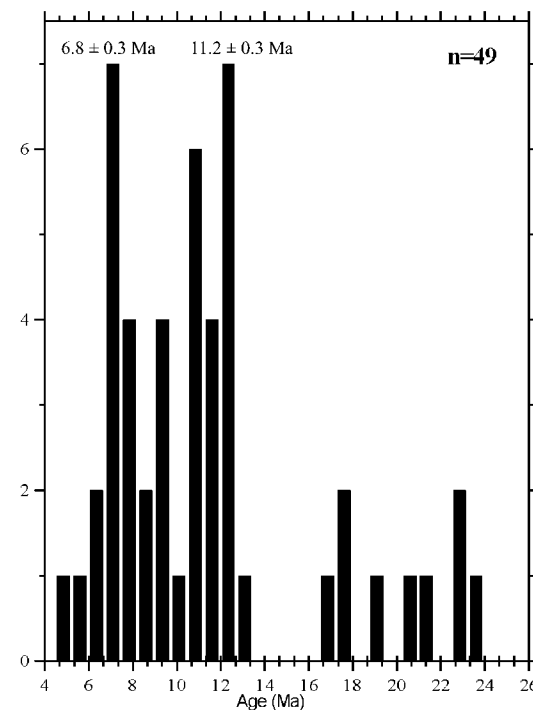


Figure 11. Histogram of all 49 Th-Pb monazite ages from Gurla Mandhata leucogranite bodies. The peaks at 7 and 11 Ma are interpreted to reflect the age of magmatic monazite. The 11 Ma year peak may also correspond to the age of metamorphic monazite. The distribution of older ages (17–24 Ma) is interpreted to reflect incorporation of inherited magmatic monazite.

0.1 Ma. The fact that the GM-4 dike cuts the GM-6 sill indicates that their crystallization ages bracket the timing of ductile shear at this position in the shear zone between 6.8 ± 0.2 Ma and 8.7 ± 0.1 Ma. However, we note that shearing must have continued at structurally higher levels in the shear zone because the unfoliated dike (GM-4) is deformed higher up in the shear zone. Nonetheless, we can assert that shearing between the dike and sill ceased by 6.8 ± 0.2 Ma because the crosscutting relationship is preserved. Monazite ages obtained from GM-5 (Table 3) yield a weighted mean age of 11.4 ± 0.1 Ma. GM-7 (Table 5) shows the widest distribution, yielding ages from early to late Miocene.

A plot of all the Th-Pb spot ages of Gurla Mandhata granite monazites reveals two distinct groups of ages at ca. 7 and 11 Ma as well as a broader distribution of ages between 17 and 24 Ma (Fig. 11). We interpret the ca. 7 and 11 Ma peaks to represent the age of magmatic monazite represented by the leuco-granite dikes and sills just discussed. Alternatively, the 11 Ma peak may reflect inheritance of metamorphic monazite grains, such as those that occur in sample GM-3, already described. The presence of 17–24 Ma ages may indicate a distinct magmatic event, as supported by extensive studies in other parts of the orogen (e.g., Schärer et al., 1986; Noble and Searle, 1995; Searle et al., 1997; Harrison et al., 1999). Alternatively, these ages may indicate incorporation of inherited magmatic monazite grains. Our interpretation of the spread of monazite ages favors inheritance of relictic grains for two reasons: (1) monazite inclusion ages from GM-3 overlap with the 11.2 Ma peak in monazite ages from the granites, and (2) monazite saturation temperatures are low. Light rare earth element concentrations (La, Ce, Pr, Nd, Sm, Gd) in samples GM-7 and GM-4 (tabulated LREE concentrations are available in the GSA Data Repository Item 3; see footnote 1) yield a monazite saturation temperature of ~ 650 °C (Rapp and Watson, 1986), which is the same as that inferred for peak metamorphic temperatures in GM-1, GM-2, and GM-3. We therefore expect these granites to contain a large number of inherited monazite grains.

$^{40}\text{Ar}/^{39}\text{Ar}$ thermochronology was conducted to characterize the time of exhumation of rocks within the footwall of the Gurla Mandhata detachment system. Ten samples were analyzed for $^{40}\text{Ar}/^{39}\text{Ar}$, of which four were collected immediately beneath the lower detachment and six were collected at structurally deeper levels (Figs. 12 and 2; GSA Data Repository Item 4; see footnote 1). All ages and

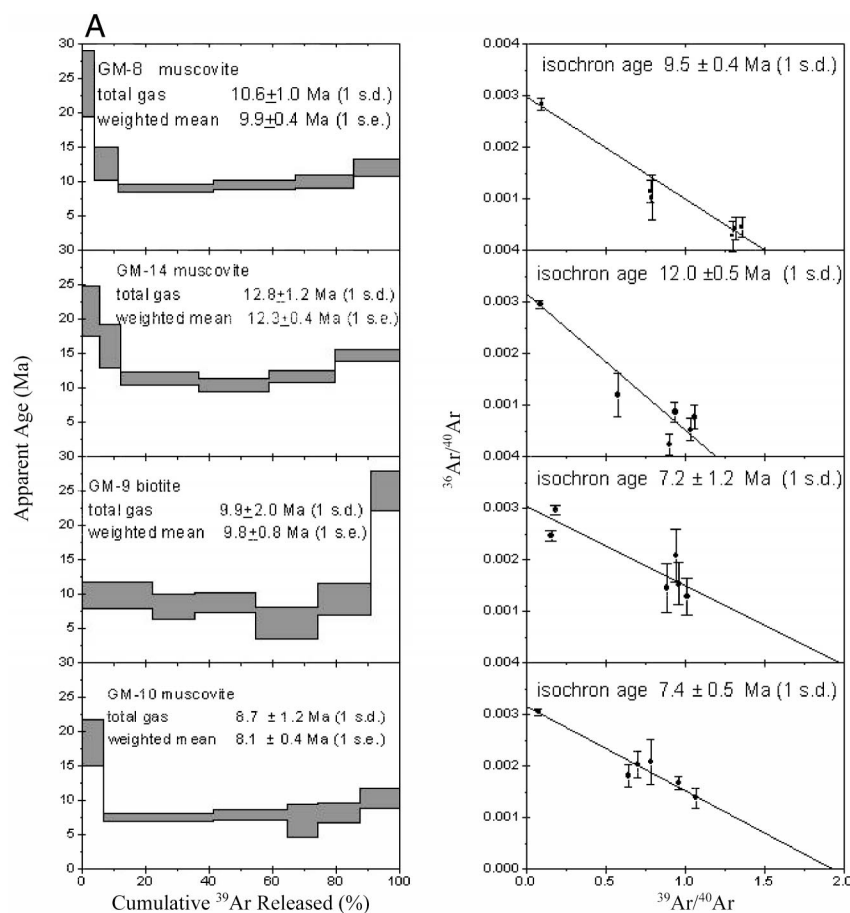


Figure 12. $^{40}\text{Ar}/^{39}\text{Ar}$ age spectra and isochron diagrams for muscovite and biotite from rocks in the footwall of the Gurla Mandhata detachment system.

isotopic ratios are reported at the 2σ uncertainty level. $^{40}\text{Ar}/^{39}\text{Ar}$ analyses were performed at UCLA on a VG3600 equipped with a quadrupole mass spectrometer. Samples were step heated to obtain three-isotope plots to correct for the composition of the trapped Ar.

Sampling and subsequent analyses were conducted to test for variations in cooling ages, both along strike and in the transport direction of the detachment system. Moreover, samples GM-8 through GM-15 were collected at an appropriate distance from granite dikes to assure that they were not significantly reheated during intrusion. All samples analyzed, regardless of location, yield late Miocene ages (Figs. 2 and 12). Samples that lie within the upper 100 m of the footwall extensional shear zone, immediately beneath Gurla Mandhata detachment fault 2 or locally beneath Gurla Mandhata detachment fault 1 (GM-8, GM-9, GM-10, GM-11), yield weighted mean ages between 9.9 and 7.4 Ma. Younger ages correspond to more northern positions along strike of the detachment system near Ronggua

gorge, possibly reflecting northward propagation of the fault system. Parallel to the transport direction of the fault, samples along Ronggua gorge (GM-12, GM-13, GM-5) show no apparent pattern in their cooling ages. Considering only the weighted mean ages of samples from Ronggua gorge suggests that the structurally deepest rocks in the footwall cooled below 400 °C by ca. 9 Ma. In two other valleys, structurally lower rocks (GM-14 and GM-15) cooled 1–2 m.y. earlier than rocks structurally above them (GM-8 and GM-11) (Fig. 2), suggesting significant telescoping due to shearing of the footwall rock.

DISCUSSION

Tectonic Evolution of the Gurla Mandhata Detachment System

Magnitude of Slip

Limits on the minimum net slip on the Gurla Mandhata detachment system are set by the extent of the ductile shear zone exposed in a direction parallel to the slip direction, which

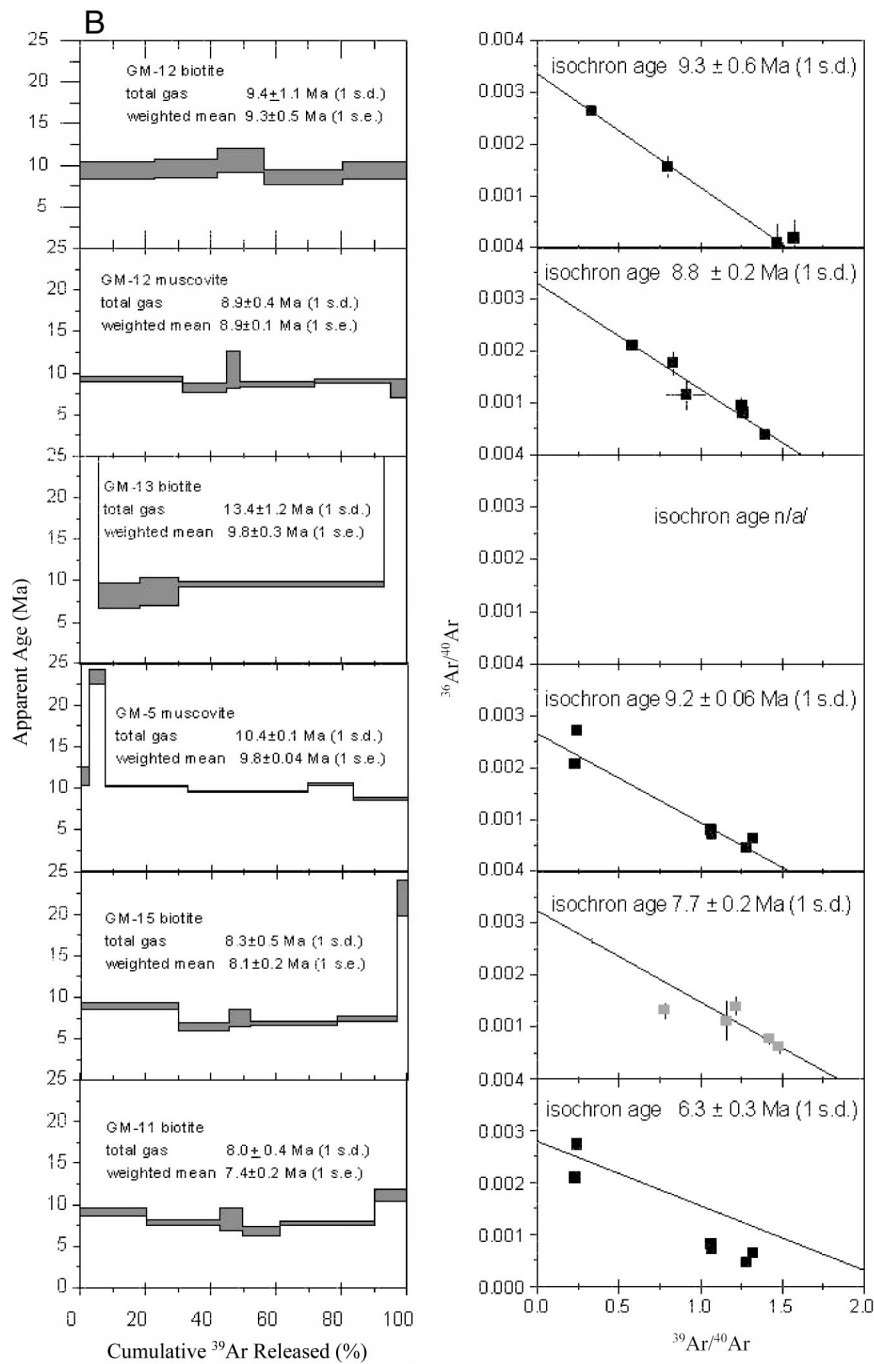


Figure 12. (Continued.)

is ~ 20 km (Figs. 2 and 6A). The maximum slip estimate is defined by the pressure estimate for sample GM-3 and GM-2. The pressure-temperature estimates for these two rocks indicate that they equilibrated at significantly different peak pressures. If a lithostatic pressure gradient of 0.27 kbar/km (average rock density of 2750 kg/m^3) is assumed, the peak pressures can be translated to depth of equilibration relative to the surface. Note that the

uncertainties in the pressure-temperature estimates represent their precision and not their accuracy, as uncertainties in the calibrations and activity models are not considered. Sample GM-2 yield depths of 18.5–28.2 km. GM-1 yields pressures between 6 and 7.2 kbar, corresponding to depths between 22.2 and 26.7 km. The pressure estimate for sample GM-3 is lower, 3.6–4.5 kbar, and corresponds to a depth of 13.3–16.7 km. The higher-pressure

rocks and the lower-pressure rocks are currently separated by ~ 500 m vertically, indicating significant tectonic juxtaposition and thinning by ductile shearing. Laterally, sample GM-2 projects along contours of the foliation (see Fig. 6A) to within 3 km of sample GM-3 in the direction of fault slip. Because both GM-2 and GM-1 are currently at similar structural levels in the footwall and have pressure-temperature estimates that overlap one another, we assume that the pressure-temperature estimate for sample GM-1 better reflects the conditions of these rocks prior to slip on the Gurla Mandhata detachment system. The preceding discussion indicates that the difference in the equilibration depths between samples GM-1 and GM-3 is 9.4 ± 5.5 km. If it is assumed that these rocks reached their present position with respect to one another along a ductile shear zone at a dip of 22° (shallowest measured dip of the structurally lower detachment fault, Gurla Mandhata detachment fault 1) (Fig. 2), a minimum of 25.9 ± 14.9 km of slip along the Gurla Mandhata detachment system is required to juxtapose these two rocks (Fig. 13). For translation of these rocks to the surface, an additional 24.7 ± 4.9 km of fault slip is required. Simply using the higher-pressure estimate from samples GM-2 and GM-1 of 6.5–7.5 kbar (24–27.7 km) requires 66 ± 5.9 km of slip on a shear zone dipping at 22° to bring them to their present position in the shear zone. These slip estimates are highly sensitive to the dip of the shear zone. If the shear zone slipped at a higher angle of 45° , the magnitude of displacement to bring the rocks to their position with respect to one another decreases to 13.3 ± 7.8 km (Fig. 13A). Moreover, to bring the deepest rocks to the surface changes the slip estimate to 34.5 ± 3.1 km. We prefer the interpretation that the shear zone slipped at an angle of $<45^\circ$, because the hanging-wall strata do not show a correlative amount of eastward tilting across the basin.

An independent estimate of the depth at which these rocks resided prior to their exhumation by the Gurla Mandhata extensional system comes from considerations of the depth of the basal thrust in the Tethyan fold-and-thrust belt, which is assumed to lie along the contact between the Tethyan Sedimentary Sequence and the rocks currently exposed in the footwall of the Gurla Mandhata detachment system. Figure 4B predicts that the depth to the basal thrust is ~ 8.3 km in the south and ~ 12.4 km in the north, relative to the present-day surface. The rocks beneath the basal thrust are now exposed in the footwall of the Gurla Mandhata detachment system. If we assume

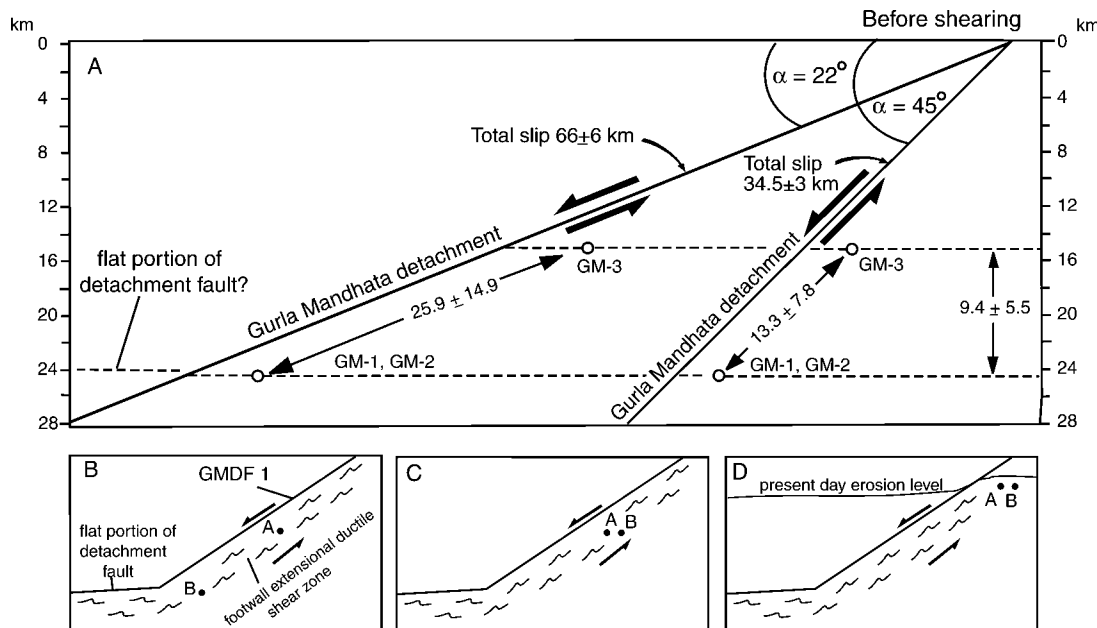


Figure 13. (A) Geometric model used to estimate magnitude of displacement along Gurla Mandhata detachment system. Estimates shown for fault dip of 22° and 45°. No vertical exaggeration. See text for explanation. (B, C, and D) Kinematic model for juxtaposition and exhumation of samples GM-3 (A) and GM-2 and GM-1 (B).

that the footwall rocks were exhumed along a fault oriented at its present dip of 22°, then 22–33 km of slip is required, corresponding to depths of 8.3 and 12.4 km, respectively. If we assume that the fault slipped at a higher angle of 45°, then the total slip changes to 12–18 km, corresponding to the same depths. To either slip estimate, 20 km must be added to account for the present exposure of the ductile extensional shear zone at the surface (Fig. 6A), increasing the slip estimate to a maximum of 53 km and a minimum of 32 km. We conclude from these different estimates that the Gurla Mandhata detachment system has accommodated at least 66 km of top-to-the-west normal shear. We view this estimate as a minimum because the detachment system may have a ramp-flat geometry (Fig. 13, B–D). In this scenario, the depth estimate of 24–27.7 km limits the minimum depth of the flat segment of the fault. Although we recognize that the Gurla Mandhata detachment system most likely does flatten at depth, we do not think that its footwall rocks have traveled far along it because of arguments for its link with the southern part of the Karakoram fault system, which is estimated to have a total of 66 km of right-slip (Murphy et al., 2000).

Structural Model

The following model views the footwall extensional shear zone, the detachment faults (Gurla Mandhata detachment faults 1 and 2),

and the Pulan basin as an evolving extensional fault system (Fig. 14). Our interpretation is largely motivated by two results of our investigation: the extensional shear zone, detachment faults, and normal faults within the Pulan basin share a common slip direction, and the crosscutting relationships and implied temperatures at which the different faults slipped are consistent with younger structures forming at successively higher levels in the crust.

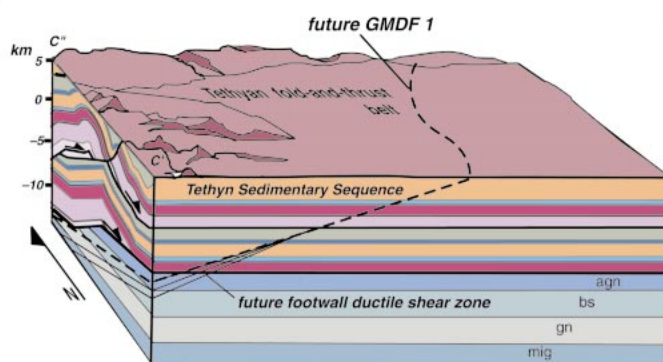
Figure 14, A–D, illustrates our interpretation. Figure 14A shows the preextensional setting whereby the Tethyan Sedimentary Sequence has been shortened by south-directed thrusts. The depth to the basal thrust based on cross section C–C' (Fig. 4B) is predicted to lie between 8.3 and 12.4 km. We interpret this as the minimum depth from which the footwall rocks of the detachment system originated prior to slip. The footwall rocks could have been subject to prograde metamorphic conditions during this early crustal thickening event. We speculate that this tectonic setting prevailed until about middle Miocene, the age of garnet crystallization. This age constraint is consistent with results reached by Yin et al. (1999b) on the age of reheating of the South Kailas thrust in the Mount Kailas area ~40 km north.

Figure 14B illustrates the initiation of Gurla Mandhata detachment fault 1 (the older detachment fault) and the extensional ductile

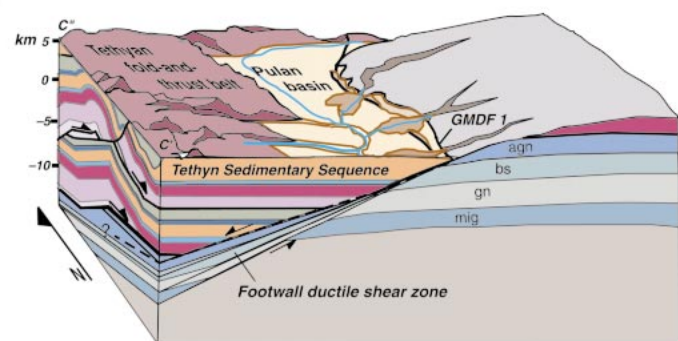
shear zone currently exposed in its footwall. We suggest that fault 1 represents the upper-crustal equivalent of the ductile shear zone. Shear along this fault system attenuated and assisted in exhumation of the footwall rocks. We rule out the possibility that fault 1 correlates with the South Tibetan detachment fault to the south of our study area (Fig. 1) on the basis of structural observations indicating that the South Tibetan detachment exhibits top-to-north shear strain (P. DeCelles, 2001, personal communication).

Figure 14C shows continued slip on Gurla Mandhata detachment fault 1; this slip translated formerly active parts of the ductile shear zone to shallower levels in the crust. Depending on what the geothermal gradient was at this time, the footwall rocks could have been exhumed to shallow enough levels in the crust to start accumulating radiogenic ^{40}Ar , implying a late Miocene age (ca. 9 Ma) for the time of slip on fault 1 and the ductile shear zone. Within the active ductile shear zone, leucogranite dikes were emplaced and subsequently sheared between 8.7 and 6.8 Ma. The correlation between the clast composition of the middle unit in the Pulan basin (Tcg2) and west- to south-directed paleoflow implies that mylonitic rocks were exposed at the surface and providing detritus to the basin. On the basis of the youngest $^{40}\text{Ar}/^{39}\text{Ar}$ mica ages of the footwall rocks on the west side of the Gurla Mandhata massif, the age of this unit is youn-

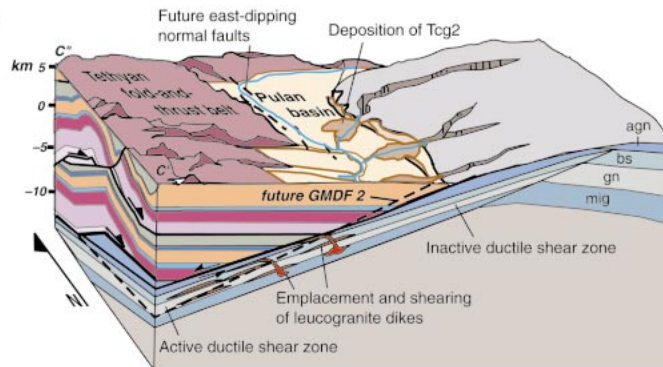
A



B



C



D

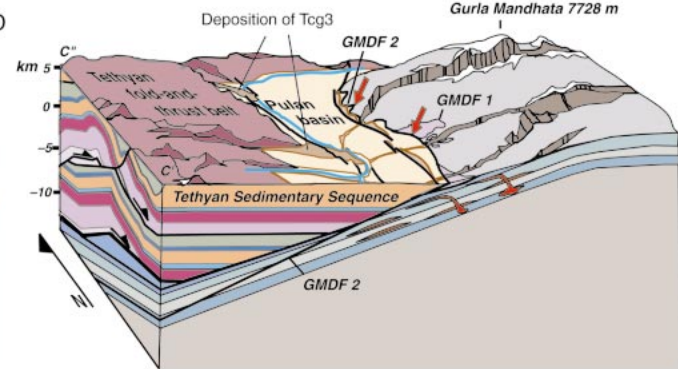


Figure 14. Structural model for the evolution of the Gurla Mandhata detachment system. (A) Preextensional setting. Tethyan Sedimentary Sequence is shortened by southward movement along thrusts belonging to the Tethyan fold-and-thrust belt, possibly resulting in prograde metamorphism of units agn, bs, gn, and mig (lithologic symbols correlate to those in Fig. 2). (B) Initiation of the footwall extensional ductile shear zone and its upper-crustal equivalent, the Gurla Mandhata detachment fault 1. (C) Continued shear on fault 1 translates formerly active parts of the ductile shear zone along with sheared leucogranite dikes to shallower levels of the crust. Deposition of Tcg2 is interpreted to have occurred at this time. (D) Initiation of Gurla Mandhata detachment fault 2 and deposition of Tcg3 possibly coeval with initiation with west-dipping normal faults within Pulan basin. Red arrows indicate the relationship where fault 2 locally cuts across fault 1, and where fault 1 has been excised by fault 2.

ger than ca. 8.1 Ma (weighted mean age of GM-10) (Fig. 12).

Figure 14D depicts the initiation of Gurla Mandhata detachment fault 2, which locally cut across Gurla Mandhata detachment fault 1 at an angle $<10^\circ$. At other localities, fault 1 has been excised by fault 2, usually at the crests of antiformal corrugations. The stratigraphically highest unit is dominated by clasts that correlate with the Tethyan Sedimentary Sequence. This change in source may reflect either eastward tilting of the hanging walls of the two Gurla Mandhata detachment faults either as domino-style tilt blocks or along a listric-shaped fault, or it may reflect uplift of the Tethyan Sedimentary Sequence in the footwall of an east-dipping normal-fault system along the western margin of the Pulan basin. We suggest that the Pulan basin represents a supradetachment basin (Friedmann and Burbank, 1995) that formed on the hanging wall of the Gurla Mandhata detachment system.

Relationship with the Karakoram Fault

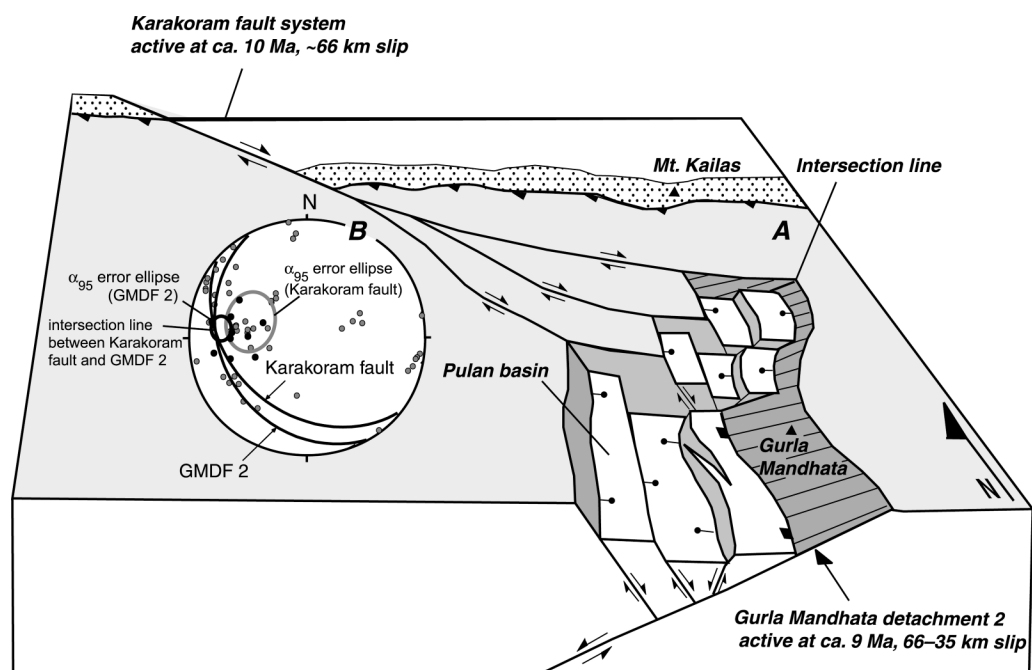
One implication of recognizing late Miocene slip on the Gurla Mandhata detachment system is that it must interact with the Karakoram fault system, which has been documented to be active at this time (Arnaud, 1992; Searle et al., 1998; Dunlap et al., 1998). We suggest that the Gurla Mandhata extensional system and the Karakoram fault system have been a kinematically linked fault system since the late Miocene on the basis of timing constraints, slip estimates, and kinematics of each fault (Fig. 15). The model we present in Figure 15 would be an example of an antithetic shear zone following terminology used by Faulds and Varga (1998).

Kinematics

South of Baer, between Menci and Mount Kailas (Fig. 1), the Karakoram fault system is represented by a broad (<45 km wide) system

of right-slip faults (Ratschbacher et al., 1994; Murphy et al., 2000) with a mean orientation of $310^\circ/35^\circ\text{SW}$ (Fig. 15). This fault system extends into the Mapam Yum Co area cutting obliquely across the Tethyan Sedimentary Sequence where it meets north-trending brittle normal faults belonging to the Gurla Mandhata detachment system. Although the intersection of the two fault systems was not recognized in the field, we suggest that the two intersect in the Mapam Yum Co area. In order for two faults to be kinematically compatible, either their principal strain axes must lie parallel to one another (Marrett and Allmendinger, 1990), or slip on both faults must be parallel to their intersection line. The latter case is true for the Karakoram fault system and the Gurla Mandhata detachment system. Figure 15 shows a plot of the mean orientation of right-slip faults between Menci and Mapam Yum Co and the orientation of Gurla Mandhata detachment fault 2 along with striations

Figure 15. (A) Kinematic model of linkage between the Karakoram fault system and the Gurla Mandhata detachment system. Our proposed model shows a system of faults that feed right-slip motion into north-striking normal faults, forming a series of pull-apart basins. The magnitude of throw along the normal faults increases from north to south as the right-slip fault system is traversed. This change explains how little denudation is observed near Mapam Yum Co, but significant denudation is observed near Gurla Mandhata. (B) Lower-hemisphere, equal-area stereonet showing the mean fault planes for the Karakoram fault system and Gurla Mandhata detachment 2 along with striations measured on individual faults (Fig. 7). As shown by the plot, the close spatial relationship between the mean slip direction on both faults and their intersection line suggests kinematic compatibility.



measured on the individual fault planes. The α_{95} error ellipses of the mean slip direction of both faults overlap and plot close to their intersection line. Ratschbacher et al. (1994) reached a similar conclusion for kinematic relationships between the Karakoram fault system and normal faults associated with the Pulan basin. Our measurements extend their conclusion to include the larger-magnitude extensional faults bounding the Gurla Mandhata massif.

Timing

Normal-slip shear on the Gurla Mandhata detachment system can be demonstrated to have occurred between 8.7 and 6.8 Ma. Age constraints on the southern segment of the Karakoram fault system can be inferred from the age of the South Kailas thrust. $^{40}\text{Ar}/^{39}\text{Ar}$ results from a K-feldspar separate from a volcanic-rock cobble in the Kailas conglomerate immediately below the thrust yield an age spectrum that is consistent with a reheating event at 13 Ma, which Yin et al. (1999b) interpreted to be due to burial by the South Kailas thrust. Because the Karakoram fault system cuts the South Kailas thrust (Murphy et al., 2000), this result places an upper age limit on the southern part of the Karakoram fault at this location. K-feldspar from a single leucogranite sample collected along the Karakoram fault system in the Zhaxigang area (~80 km north of Namru, northwest corner of Fig. 1) yields an age spectrum that indicates the rock was

rapidly cooled by ca. 10 Ma (Arnaud, 1992). Our field mapping of this area suggests that rapid cooling of these rocks may best be explained by either oblique slip along the Karakoram fault system or exhumation at a right-stepping bend in the master fault.

Displacement

Although it has been argued that the Karakoram fault system may have accommodated ~1000 km of right-slip in the Cenozoic (e.g., Peltzer and Tapponnier, 1988), a growing body of field data suggests much smaller displacements, ~250 km (Ratschbacher et al., 1994), <150 km (Searle, 1996; Searle et al., 1998), and ~66 km (Murphy et al., 2000). As discussed earlier, the magnitude of normal slip accommodated by the Gurla Mandhata detachment system is >66 km.

On the basis of these kinematic, timing, and displacement constraints for the Karakoram and the Gurla Mandhata systems, we infer that they are linked and together represent a single fault system that has been active since the late Miocene (Fig. 15). If this interpretation is valid, a consequence of the observation that the Gurla Mandhata detachment system exhumes mid-crustal rocks is that the Karakoram fault system extends to a similar crustal depth. This interpretation is supported by field and analytical investigations of migmatitic rocks exhumed along the central part of the Karakoram fault in the Banggong Co area, approximately 300 km northwest of Namru, (Fig. 1) by Sear-

le et al. (1998) and Dunlap et al. (1998). Moreover, this interpretation implies that the Karakoram fault system steps southward 90–50 km south of Mount Kailas area via the Gurla Mandhata detachment system and extends eastward into the High Himalaya of far-western Nepal as a major crustal-scale right-slip shear zone.

CONCLUSIONS

Field mapping along with geochronologic and thermobarometry analyses of the Gurla Mandhata area in southwest Tibet reveals major east-west extension along a normal-fault system, termed the “Gurla Mandhata detachment system.” The maximum structural throw occurs along a pair of low-angle normal faults (detachment faults), which juxtapose Tertiary sedimentary rocks and Paleozoic rocks belonging to the Tethyan Sedimentary Sequence in its hanging wall against amphibolite-facies mylonitic schist, marble, gneisses, and variably deformed leucogranite bodies in its footwall. Upper Tertiary strata were deposited unconformably on the Paleozoic section and are intimately associated with east- and west-dipping brittle normal faults. The footwall of the detachment faults records a late Miocene intrusive event, in part contemporaneous with top-to-the-west ductile normal shearing. Macro- and microscale sheared mylonitic rocks define a >2.1-km-thick ductile shear zone in the footwall. The consistency of the mean

shear direction within the mylonitic footwall rocks and its correlation with structurally higher brittle normal faults suggest that the faults and ductile shear zone represent an evolving low-angle normal-fault system. $^{40}\text{Ar}/^{39}\text{Ar}$ data from muscovite and biotite from the footwall rocks indicate that they cooled below 400 °C at ca. 9 Ma. Considerations of the depth at which the footwall rocks originated, prior to their exhumation along the normal-fault system, and the angle at which the fault originally dipped, yield total slip estimates between 66 and 35 km. These slip estimates and timing constraints on the Gurla Mandhata detachment system are comparable to those estimated on the right-slip Karakoram fault system. Moreover, the mean shear-sense direction on both the Karakoram fault and the Gurla Mandhata detachment system overlap along the intersection line between the mean orientation of the faults and suggest that the two are kinematically linked. If valid, this interpretation reinforces previous data suggesting that the Karakoram fault extends to mid-crustal depths, as indicated by the exhumation of amphibolite-facies mylonitic rocks along the Gurla Mandhata detachment system. Ratschbacher et al. (1994) reached a similar conclusion between the Karakoram fault system and normal faults associated with the Pulan basin. Our measurements extend their conclusion to include the larger magnitude extensional faults represented by the Gurla Mandhata detachment faults. If valid, this interpretation reinforces previous data suggesting that the Karakoram fault extends to mid-crustal depths, as indicated by exhumation of amphibolite-facies mylonitic rocks along the Gurla Mandhata detachment system.

ACKNOWLEDGMENTS

We thank Richard Law, Laurent Godin, and Mike Searle for thorough reviews, which greatly improved the manuscript. This work was supported by National Science Foundation grant EAR-9628178 (to An Yin and T.M. Harrison) and Lawrence Livermore National Laboratory grant 97-GS-001 (to An Yin and T.M. Harrison).

REFERENCES CITED

- Allègre, C.J., Courtillot, V., Tapponier, P., Hirn, A., Matrauer, M., Coulon, C., Jaeger, J.J., Achache, J., Schaeffer, Urs, Marcoux, J., Burg, J.P., Girardeau, J., Armijo, R., Gariepy, C., Goepel, C., Li Tindong, Xiao Xuchang, Chang Chenfa, Li Guangjin, Lin Baoyu, Teng Ji Wen, Wang Naiwen, Chen Guoming, Han Tonglin, Wang Xibin, Den Wanming, Sheng Huaibin, Cao Yougong, Zhou Ji, Qiu Hongrong, Bao Peisheng, Wang Songchan, Wang Bixiang, Zhou Yaoxiu, and Ronghua Xu, 1984, Structure and evolution of the Himalayan-Tibet orogenic belt: *Nature*, v. 307, p. 17–22.
- Armijo, R., Tapponier, P., and Han, T., 1989, Late Cenozoic right-lateral strike-slip faulting in southern Tibet: *Journal of Geophysical Research*, v. 94, p. 2787–2838.
- Arnaud, N.O., 1992, *Apports de la thermochronologie $^{40}\text{Ar}/^{39}\text{Ar}$ sur feldspath potassique à la connaissance de la tectonique Cénozoïque d'Asie* [Ph.D. thesis]: Paris, Université Blaise Pascal, 160 p.
- Aouac, J.-P., and Tapponier, P., 1993, Kinematic model of active deformation in central Asia: *Geophysical Research Letters*, v. 20, p. 895–898.
- Brookfield, M.E., 1993, The Himalayan passive margin from Precambrian to Cretaceous: *Sedimentary Geology*, v. 84, p. 1–35.
- Burchfiel, B.C., Chen Zhiliang, Hodges, K.V., Liu Yiping, Royden, L.H., Deng, C., and Xu, J., 1992, The south Tibetan detachment system, Himalayan orogen: Extension contemporaneous with and parallel to shortening in a collisional mountain belt: *Geological Society of America Special Paper* 269, 41 p.
- Burg, J.-P., and Chen, G.M., 1984, Tectonics and structural formation of southern Tibet, China: *Nature*, v. 311, p. 219–223.
- Burtman, V.S., and Molnar, P., 1993, Geological and geophysical evidence for deep subduction of continental crust beneath the Pamir: *Geological Society of America Special Paper* 281, 76 p.
- Chang Chengfa, Chen Nansheng, Coward, M.P., Deng Wanming, Dewey, J.F., Gansser, A., Harris, N.B.W., Jin Chengwei, Kidd, William S.F., Leeder, M.R., Li Huan, Lin Jinlu, Liu Chengjie, Mei Houjun, Molnar, P., Pan Yun, Pan Yusheng, Pearce, Julian A., Shackleton, R.M., Smith, A.B., Sun Yiyin, Ward, M., Watts, D.R., Xu Juntao, Xu Ronghua, Yin Jixiang, and Zhang Yuquan, 1986, Preliminary conclusions of the Royal Society and Academia Sinica 1985 geotraverse of Tibet: *Nature*, v. 323, p. 501–507.
- Chen, W., and Molnar, P., 1983, Focal depths of intracontinental and intraplate earthquakes and their implications for the thermal and mechanical properties of the lithosphere: *Journal of Geophysical Research*, v. 88, p. 4183–4214.
- Cheng, J., and Xu, G., 1987, Geologic map of the Gerdake region at a scale of 1:1000000 and geologic report: Xizang Bureau of Geology and Mineral Resources, 363 p. (in Chinese).
- Corfield, R.I., and Searle, M.P., 2000, Crustal shortening estimates across the north Indian continental margin, Ladakh, northwest India, in Khan, M.A., Treloar, P.J., Searle, M.P., and Jan, M.Q., eds., *Tectonics of the Nanga Parbat syntaxis and the Western Himalaya: Geological Society [London] Special Publication* 170, p. 395–410.
- DeCelles, P.G., Gehrels, G.E., Quade, J., LaReau, B., and Spurlin, M., 2000, Tectonic implications of U-Pb zircon ages of the Himalayan orogenic belt in Nepal: *Science*, v. 288, p. 497–499.
- Dunlap, W.J., Weinberg, R.F., and Searle, M.P., 1998, Karakoram fault zone rocks cool in two phases: *Geological Society [London] Journal*, v. 155, p. 903–912.
- England, P., and Molnar, P., 1997, Active deformation of Asia: From kinematics to dynamics: *Science*, v. 278, p. 647–650.
- Faulds, J.E., and Varga, R.J., 1998, The role of accommodation zones and transfer zones in the regional segmentation of extended terranes, in J.E., Faulds and J.H. Stewart, eds., *Accommodation zones and transfer zones: The regional segmentation of the Basin and Range province: Geological Society of America Special Paper* 323, p. 1–45.
- Ferry, J.M., and Spear, F.S., 1978, Experimental calibration of the partitioning of Fe and Mg between biotite and garnet: *Contributions to Mineralogy and Petrology*, v. 66, p. 113–117.
- Florence, F.P., and Spear, F.S., 1992, Effects of diffusional modification of garnet growth zoning on P-T path calculations: *Contributions to Mineralogy and Petrology*, v. 107, p. 487–500.
- Friedmann, S.J., and Burbank, D.W., 1995, Rift basins and supradetachment basins: Intracontinental extensional end-members: *Basin Research*, v. 7, p. 109–127.
- Gansser, A., 1964, *The geology of the Himalayas*: New York, Wiley Interscience, 289 p.
- Garzanti, E., 1999, Stratigraphy and sedimentary history of the Nepal Tethys Himalaya passive margin: *Journal of Asian Earth Sciences*, v. 17, p. 805–827.
- Girardeau, J., Marcus, J., Allègre, C.J., Bassoulet, J.P., Tang, Y., Xiao, X., Cao, Y., and Wang, S., 1984, Tectonic environment and geodynamic significance of the Neo-Cimmerian Dongqiao ophiolite, Bangong-Nujiang suture zone, Tibet: *Nature*, v. 307, p. 27–31.
- Harrison, T.M., McKeegan, K.D., and LeFort, P., 1995, Detection of inherited monazite in the Manaslu leucogranite by $^{208}\text{Pb}/^{232}\text{Th}$ ion microprobe dating: Crystallization age and tectonic implications: *Earth and Planetary Science Letters*, v. 133, p. 271–282.
- Harrison, T.M., Grove, M., McKeegan, K.D., Coath, C.D., Lovera, O.M., and LeFort, P., 1999, Origin and emplacement of the Manaslu intrusive complex, Central Himalaya: *Journal of Petrology*, v. 40, p. 3–19.
- Heim, A., and Gansser, A., 1939, Central Himalaya, geological observations of the Swiss expeditions 1936: *Mémoire Société Helvétique Science. Naturelle*, v. 73, p. 1–245.
- Hodges, K.V., 2000, Tectonics of the Himalaya and southern Tibet from two perspectives: *Geological Society of America Bulletin*, v. 112, p. 324–350.
- Holdaway, M.J., 1971, Stability of andalusite and the aluminum silicate phase diagram: *American Journal of Science*, v. 271, p. 97–131.
- Holland, T.B., and Powell, R., 1998, An internally consistent thermodynamic data set for phases of petrologic interest: *Journal of Metamorphic Petrology*, v. 16, p. 309–344.
- Klootwijk, C.T., Conaghan, P.J., Nazirullah, R., and de Jong, K.A., 1992, Further palaeomagnetic data from Chitral (eastern Hindukush): Evidence for an early India-Asia contact: *Tectonophysics*, v. 237, p. 1–25.
- Kozloli, A.M., and Newton, R.C., 1988, Redetermination of the anorthite breakdown reaction and improvement of the plagioclase-garnet-Al₂SiO₅-quartz (GASP) barometer: *American Mineralogist*, v. 73, p. 216–223.
- Liu, Q., 1993, *Paléoclimat et contraintes chronologiques sur les mouvements récents dans l'ouest du Tibet: Failles du Karakorum et de Longmu Co-Gozha Co, lac en pull-apart de Longmu Co et de Sumxi Co* [Ph.D. thesis]: Paris, Université de Paris 7, 360 p.
- Marrett, R., and Allmendinger, R.W., 1990, Kinematic analysis of fault-slip data: *Journal of Structural Geology*, v. 12, p. 973–986.
- McCaffrey, R., and Nabelek, J., 1998, Role of oblique convergence in the active deformation of the Himalayas and southern Tibet plateau: *Geology*, v. 26, p. 691–694.
- Miller, C., Schuster, R., Klotzli, U., Frank, W., and Purtscheller, F., 1999, Post-collisional potassio and ultra-potassio magmatism in southwest Tibet: Geochemical and Sr-Nd-Pb-O isotopic constraints for mantle source characteristics and petrogenesis: *Journal of Petrology*, v. 40, p. 1399–1424.
- Molnar, P., and Lyon-Caen, H., 1989, Fault plane solutions of earthquakes and active tectonics of the Tibetan plateau and its margins: *Geophysical Journal International*, v. 99, p. 123–153.
- Molnar, P., England, P., and Martinod, J., 1993, Mantle dynamics, uplift of the Tibetan plateau, and the Indian monsoon: *Review of Geophysics*, v. 31, p. 357–396.
- Murphy, M.A., Yin, A., Harrison, T.M., Durr, S.B., Chen, Z., Ryerson, F.J., Kidd, W.S.F., Wang, X., and Zhou, X., 1997, Did the Indo-Asian collision alone create the Tibetan plateau?: *Geology*, v. 25, p. 719–722.
- Murphy, M.A., Yin, A., Kapp, P., Harrison, T.M., Ding, L., and Guo, J., 2000, Southward propagation of the Karakoram fault system, southwest Tibet: Timing and magnitude of slip: *Geology*, v. 28, p. 451–454.
- Noble, S.R., and Searle, M.P., 1995, Age of crustal melting and leucogranite formation from U-Pb zircon and monazite dating in the Western Himalaya, Zanskar, India: *Geology*, v. 23, p. 1135–1138.
- Parrish, R.R., and Hodges, K.V., 1996, Isotopic constraints on the age and provenance of the Lesser and Greater Himalayan sequences, Nepalese Himalaya: *Geological Society of America Bulletin*, v. 108, p. 904–911.
- Pearce, J.A., and Deng, W., 1988, The ophiolites of the Tibetan geotraverse, Lhasa-Golmud (1985) and Lhasa

- to Kathmandu (1986): Royal Society of London Philosophical Transactions, v. A327, p. 215–238.
- Pêcher, A., 1991, The contact between the Higher Himalaya crystallines and the Tibetan sedimentary series: Miocene large-scale dextral shearing: *Tectonics*, v. 10, p. 587–598.
- Peltzer, G., and Tapponnier, P., 1988, Formation and evolution of strike-slip faults, rifts, and basins during the India-Asia collision: An experimental approach: *Journal of Geophysical Research*, v. 93, p. 15085–15117.
- Powell, R., and Holland, T., 1988, An internally consistent data set with uncertainties and correlations: 3. Applications to geobarometry, worked examples and a computer program: *Journal of Metamorphic Petrology*, v. 6, p. 173–204.
- Rapp, R.P., and Watson, E.B., 1986, Monazite solubility and dissolution kinetics: Implications for the thorium and light rare earth chemistry of felsic magmas: Contributions to Mineralogy and Petrology, v. 94, p. 304–316.
- Ratschbacher, L., Frisch, W., and Liu, G., 1994, Distributed deformation in southern and western Tibet during and after the India-Asia collision: *Journal of Geophysical Research*, v. 99, p. 19917–19945.
- Rowley, D.B., 1996, Age of collision between India and Asia: A review of the stratigraphic data: *Earth and Planetary Science Letters*, v. 145, p. 1–13.
- Rutter, E.H., Maddock, R.H., Hall, S.H., and White, S.H., 1986, Comparative microstructures of natural and experimentally produced clay-bearing fault gouges: *Pure and Applied Geophysics*, v. 124, p. 3–30.
- Schärer, U., Xu, R., and Allègre, C.J., 1986, U-(Th)-Pb systematics and ages of Himalayan leucogranites, south Tibet: *Earth and Planetary Science Letters*, v. 77, p. 35–48.
- Searle, M.P., 1996, Geological evidence against large-scale pre-Holocene offsets along the Karakoram fault: Implications for the limited extrusion of the Tibetan plateau: *Tectonics*, v. 15, p. 171–186.
- Searle, M.P., Parrish, R.R., Hodges, K.V., Hurford, A., Ayres, M.W., and Whitehouse, M.J., 1997, Shisha Pangma leucogranite, south Tibetan Himalaya: Field relations, geochemistry, age, origin, and emplacement: *Journal of Geology*, v. 105, p. 295–317.
- Searle, M.P., Weinberg, R.F., and Dunlap, W.J., 1998, Transpressional tectonics along the Karakoram fault zone, northern Ladakh: Constraints on Tibetan extrusion, in Holdsworth, R.E., et al., eds., *Continental transpressional and transtensional tectonics: Geological Society [London] Special Publication 135*, p. 307–326.
- Seeber, L., and Pêcher, A., 1998, Strain partitioning along the Himalayan arc and the Nanga Parbat antiform: *Geology*, v. 26, p. 791–794.
- Senjō A.M.C., and Natal'in, B.A., 1996, Paleotectonics of Asia: Fragments of a synthesis, in Yin, A., and Harrison, T.M., eds., *The tectonic evolution of Asia*: Cambridge, UK, Cambridge University Press, p. 486–640.
- Smith, H.A., and Giletti, B.J., 1997, Lead diffusion in monazite: *Geochimica et Cosmochimica Acta*, v. 61, p. 1047–1055.
- Spear, F.S., 1993, Metamorphic phase equilibria and pressure-temperature-time paths: Washington, D.C., Mineralogical Society of America, 799 p.
- Strecker, M.R., Frisch, W., Hamburger, M.W., Ratschbacher, L., Semiletkin, S., Zamoruyev, A., and Sturchio, N., 1995, Quaternary deformation in the eastern Pamirs, Tadzhikistan and Kyrgyzstan: *Tectonics*, v. 14, p. 1061–1079.
- Tapponnier, P., Mattauer, M., Proust, F., and Cassaigneau, C., 1981, Mesozoic ophiolites, sutures, and large-scale tectonic movements in Afghanistan: *Earth and Planetary Science Letters*, v. 52, p. 355–371.
- Tapponnier, P., Peltzer, G., Le Dain, A.Y., and Armijo, R., 1982, Propagating extrusion tectonics in Asia: New insights from simple experiments with plasticine: *Geology*, v. 10, p. 611–616.
- Yin, A., 1991, Mechanisms for the formation of the domal and basinal detachment faults: A three-dimensional analysis: *Journal of Geophysical Research*, v. 96, p. 14577–14594.
- Yin, A., and Harrison, T.M., 2000, Geologic evolution of the Himalayan-Tibetan orogen: *Annual Review of Earth and Planetary Sciences*, v. 28, p. 211–280.
- Yin, A., and Nie, S., 1996, A Phanerozoic palinspastic reconstruction of China and its neighboring regions, in Yin, A., and Harrison, T.M., eds., *The tectonic evolution of Asia*: Cambridge, UK, Cambridge University Press, p. 442–485.
- Yin, J., Xu, J., Liu, C., and Li, H., 1988, The Tibetan plateau: Regional stratigraphic context and previous work: Royal Society of London Philosophical Transactions, v. A327, p. 5–52.
- Yin, A., Kapp, P.A., Murphy, M.A., Harrison, T.M., Grove, M., Ding, L., Deng, X.-G., and Wu, C.-M., 1999a, Significant late Neogene east-west extension in northern Tibet: *Geology*, v. 27, p. 787–790.
- Yin, A., Harrison, T.M., Murphy, M.A., Grove, M., Nie, S., Ryerson, F.J., Wang, X., and Chen, Z., 1999b, Tertiary deformation history in southeastern and southwestern Tibet during the Indo-Asian collision: *Geological Society of America Bulletin*, v. 111, p. 1644–1664.

MANUSCRIPT RECEIVED BY THE SOCIETY SEPTEMBER 25, 2000

REVISED MANUSCRIPT RECEIVED AUGUST 22, 2001

MANUSCRIPT ACCEPTED SEPTEMBER 26, 2001

Printed in the USA